ADDIS ABABA UNIVERSITY

ADDIS ABABA INSTITUTE OF TECHNOLOGY

SCHOOL OF MECHANICAL AND INDUSTRIAL ENGINEERING

Effect of Curved Track on Rolling Contact Fatigue at Wheel-Rail Interface in Addis Ababa Light Rail Transit

By

Aregay Haile

A Thesis Submitted to the Graduate School of Addis Ababa University in Partial Fulfillment of the Requirements for the Degree of Masters of Science

In

Mechanical Engineering

(Under Railway Engineering)

Advisor

Ato Habtamu Tkubet (MSc)

May, 2015

AKNOWLEDGEMENT

First of all, I am very delightful to praise the Almighty God who has enabled me to complete my thesis work. Next, I would like to thank my MSc. Thesis Advisor Mr. Habtamu Tkubet for his support and guidance. And I would like to express my gratitude to Ethiopian Railway Corporation (ERC) for providing me the opportunity to study in Railway Engineering. And also I would like to thank to Addis Ababa light rail transit (AA LRT) project office for their cooperation to do my thesis. They gave me valuable information about AA LR track conditions and vehicle specifications as well as provided me the necessaries data and specifications. Lastly, I extend my sense of gratitude to all my friends who directly or indirectly helped me in my thesis work.

ABSTRACT

The thesis presents analysis of rolling contact fatigue at the wheel-rail interface using FEM. The aim of the thesis is to determine the stress/strain and predict the fatigue life at the wheel-rail rolling contact by considering the effect of rolling contact coefficient of friction and track conditions. For this thesis the outer wheel is taken for FEA model. A three-dimensional elastic-plastic finite element model of the wheel-rail rolling contact is used to investigate the effect of coefficient of friction and track conditions. The loading and boundary conditions of the wheel-rail rolling contact is accurately shown by the FE ANSYS simulation. The FE fatigue analysis is based on the stress life analysis. The effect of mean stress correction is considered in the analysis. The effect of rolling contact friction coefficient and track conditions are also investigated in detail using the FEA. The obtained results show that the friction coefficient at the wheel-rail contact has significant effect on the fatigue life at the wheel-rail rolling contact and track condition has a large effect on the fatigue crack initiation and in all cases the minimum fatigue life is indicated at the rail rolling contact. The obtained maximum equivalent alternating stresses at the rail rolling contact at constant coefficient of friction, ($\mu = 0.15$) at different track conditions (at straight, transition and circular curve track paths) are 278.24Mpa, 292.7Mpa, 384.81Mpa, The results are very useful for wheel-rail rolling contact fatigue resistance design, inspection and maintenance for Addis Ababa light rail transit in Ethiopia.

Key words: Wheel-rail rolling contact fatigue (RCF), track conditions (straight, transition curve, circular curve track), rolling contact coefficient of friction, stress-life and fatigue life.

Table of Contents

SYMBOLS AND ABBREVIATIONS

FEM	Finite element method
FEA	Finite element analysis
RCF	Rolling contact fatigue
AA LRT	Addis Ababa light rail transit
UIC	International union of railways
COF	Coefficient of friction
σ	Stress
σ_y	Yield stress
σ_{El}	Elastic limit of the stress
σ_{Pl}	Plastic limit of the stress
F_N	Normal contact force
F_{NLw}	Normal contact force at the left wheel
F_{NRw}	Normal contact force at the right wheel
W	Axle weight
m	Axle mass
g	Gravitational acceleration constant
2l	The lateral distance between wheelset contacts
δ	Wheel conicity
y	Lateral displacement
r	Normal rolling radius of the wheel

r_{inner}	Inner rolling contact radius of the wheel during curving
r_{outer}	Outer rolling contact radius of the wheel during curving
R	Radius of curvature
V	Tangential velocity of the vehicle
a_c	Centripetal acceleration
F_c	Centrifugal force
S	Superelevation height
Φ	Superelevation angle or track cant angle
F^t_{Lw}	Lateral contact force at the tread left wheel
F^t_{Rw}	Lateral contact force at the tread right wheel
F^f_{Rw}	Lateral flange force at the right wheel
F_g	Gravitational force
Q_{Rw}	Vertical force at the right wheel
μ	Coefficient of friction
Ɵ	Angle associated to the sets of forces acting on the left wheel
α	Angle associated to the sets of forces acting on the right wheel
β	Rail inclination angle
L	Total transition curve length
l_p	Length at any point of the transition curve
R	Circular curve radius
r_p	Curve radius at any point of the transition length
K	Constant
LCF	Low cycle fatigue

HCF	High cycle fatigue
b	Fatigue strength exponent
S-N	Stress-life
$\Delta\sigma/2 = \sigma_a$	Stress amplitude
σ_{alt}	alternating stress
σ_{mean}	Mean stress
$S_{End\text{-}limt}$	Endurance limit
$S_{Ult\text{-}strength}$	Ultimate strength

LIST OF FIGURES

LIST OF TABLES

CHAPTER ONE

INTRODUCTION

1.1. Back ground

1.1.1. Rail transportation in Ethiopia

Since the first iron track was developed in 1738[1], railways have been playing an important role in public transportation. In Ethiopia, The first rail transportation (train service) began on July 22, 1901, and operated between Djibouti and Douala, the first station on the Ethiopian side of the frontier at kilometer 106, a journey of 5 1/2 hours [2]. By 1915 the line reached Akaki, only 23 kilometers from the capital city, and two years later came all the way to Addis Ababa itself [3]. This marked the official commercial opening of the 784 km long railway although the Station of Addis Ababa was not inaugurated until 3 December 1929. For many years the railway operation was interrupted. Now the railway is currently being rebuilt and electrified by Chinese and Turkish companies. It is scheduled to be completed by September, 2015. And will be 756 km in length. The new railroad is expected to reduce the travel time from Addis Ababa to Djibouti by half to less than ten hours with a designated speed of 120 km/h [4]. Additionally, Addis Ababa light rail is under construction. It is constructed by china railway group limited. The Ethiopian railway corporation began construction of the 34.25 km double track electrified light rail transit project in December 2011[5]. Initially the light rail system will have two lines. The east-west line will extend 17.35 km which is stretching from Ayat village to the gate of Tor hailoch and the north-south line which will be 16.9 km in length stretching from Menelik square to Kaliti. It is expect to start operation at circa 2015 [6]. Thus, the present study focuses on Addis Ababa light rail transit real conditions and specifications.

Railway transport during the last years has increased in speed, security and comfort. In comparison to automobiles, railway transport is a more secure and less environment damaging means of transportation. In order to keep up the competiveness of railroad transportation, increasing

requirements on the speed of passenger and freight trains, on the axle load of the trains as well as the comfort of the passengers have to be met. Further pressure on the development arises from the demand of decreasing the costs of both new trains and new rail tracks as well as the maintenance costs. Thus a large number of investigations have focused an optimization of trains, rail tracks and the rail/wheel system. For instance, optimizing the rail top profile. The mechanisms of material changes at the rail-wheel interface also have received considerable attention. But, so far the structure changes that occur in the rail and the wheel material during service still have not been completely solved and clarified. In service the surface of the rail track as well as the surface of the wheel sets are subject to strong changes due to their long time sustaining load and wear. Also, efforts have been made to optimize wheel and rail design to improve the performance and reduce the cost. These trends have changed the major wheel rim damage from wear to fatigue [7].

The concept of fatigue has been known since the midst of the nineteenth century. A major literature survey which should contain all articles regarding fatigue published between 1838 and 1950 is presented by Mann [8]. In 1871, the first major systematic investigation of the phenomenon was made by Wöhler [9]. The study was initiated by the fracture of locomotive wheel axles. Since the discoveries by Wöhler, fatigue has been thoroughly studied. However, there are still several areas for which there are no satisfactory theories to explain the observed phenomena and to serve as a tool to predict fatigue behaviour. Some of these areas (e.g. multiaxial fatigue and cumulative damage) are crucial parts in the modelling of rolling contact fatigue in wheel/rail contacts. According to Lin [10], more than 90% of all catastrophic failures of structures are caused by fatigue of materials. Fatigue does, as indicated by the designation, include some sort of exhaustion of the material. This is manifested by material failure at fluctuating stress levels far below those leading to fracture at static loading. The provision is that the material is exposed to these fluctuating stress levels for a “long time”, or rather, for many cycles. The specific objective of this thesis is to predict the fatigue life at the wheel-rail rolling contact using three dimensional finite element analysis (3D FEA) ANSYS software based on Addis Ababa light rail transit real conditions and specifications. The study is very valuable for fatigue resistance design and inspection planning of wheel and rail in AA LRT (Ethiopia).

1.1.2. Wheel rolling contact fatigue (RCF)

Damage accumulation due to fatigue, plastic deformation and wear, significantly reduces the service life of the railway track [7]. In recent years, higher train speeds and increased axle loads have led to larger wheel/rail contact forces. Also, efforts have been made to optimize wheel and rail design. This evolution tends to change the major wheel rim damage from wear to fatigue [7]. Unlike the slow deterioration process of wear, fatigue causes abrupt fractures in wheels or the tread surface material loss. These failures may cause damage to rails, damage to train suspensions and, in rare cases, serious derailment of the train. The fatigue problem of railroad wheels is often referred to as rolling contact fatigue [30], which is caused by repeated contact stress during the rolling motion. The proper understanding of the underlying mechanism of rolling contact fatigue requires detailed knowledge of the interaction between wheel and rail. A proper multiaxial fatigue damage accumulation model under complex rolling contact stress state is also required.

Railroad wheels may fail in different ways corresponding to different failure mechanisms [31-33]. Ekberg A, Marais J, [34] divide the wheel fatigue failure modes into three different failure types corresponding to different initiation locations. Surface initiated, subsurface initiated and deep surface initiated fatigue failures. On the tread surface, there are usually two types of cracks. One is caused by the repeated mechanical contact stress. The other is initiated by thermal stresses arising from on-tread friction braking. But, this thesis focuses on rolling contact fatigue damage due to repeated mechanical contact stress.

Surface initiated fatigue: initiation of surface cracks is related to plastic deformation of the material in the surface layer of the wheel rim. The main cause of global plastic deformation of the surface material is the applied interfacial shear stress between the wheel tread and the rail head. Surface initiated RCF cracks are more common, but less severe than sub surface initiated RCF cracks on a wheel fleet. The loading is likely to be lower than what is optimum from an economical point of view. Still, this is a delicate balance. When the loading (in a broad sense) is increased above a certain level, an epidemic of surface initiated cracks will occur with cracking frequencies and severity exceeding acceptable levels.

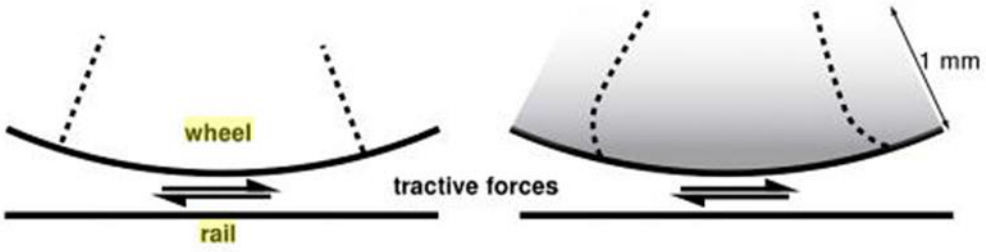

Figure 1.1: Schematic sketch of plastic deformation of the surface material in a railway wheel. The dashed line indicates material planes before and after deformation [11].

Sub surface initiated fatigue: sub-surface initiated RCF cracks are rare, but the consequences are often severe. In a worst case scenario the train may derail, but also when the train does not derail the impact of the cracked wheel may cause significant damage to both rail and bogie. Therefore, to understand the mechanisms behind surface initiated RCT we need to understand both the contact mechanics and the mechanisms behind fatigue crack initiation and growth.

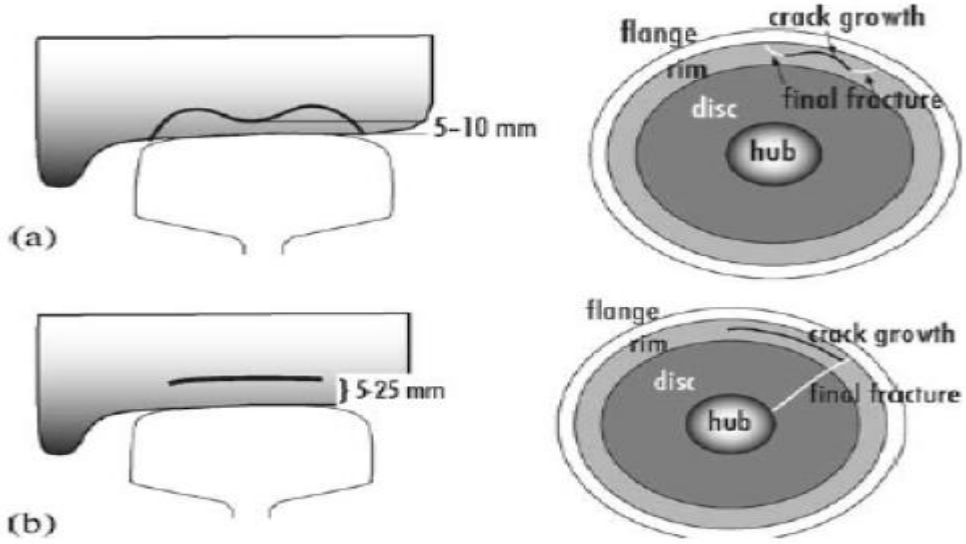

Figure 1.2: Typical appearance of sub surface fatigue cracks in railway wheels.(a) shallow initiation, (b) deep initiation [11].

1.1.3. Rail rolling contact fatigue (RCF)

Rolling Contact Fatigue (RCF) in rails was known in the late 1990s [19] but was underestimated. Now, with the high speed, dense traffic and high axle loads of modern railways, RCF has become a more serious problem highlighted by the Hatfield train disaster [14]. Factors affecting RCF are rail curve radius, wheel base, wheel diameter, axle load, primary yaw stiffness of suspension, rail-wheel profiles, traction, braking forces and rail-wheel material property [17]. RCF is traditionally known (and recognized) by its surface manifestations and was widely known as 'squat' in Britain and in Japan as 'black spot'. RCF is associated with plastic deformation under contact forces and a crack initiates due to a unidirectional accumulation of strain that propagates downward under successive applications of compressive contact stresses. Oliver [20] explains that, if the contacting bodies are smooth, loaded below the elastic limit and not subjected to any tractive forces, then the stress field near the contact is just that due to the Hertz pressure distribution. This may also even be true if the contacting surfaces are not perfectly smooth but are lubricated with oil giving a film thickness that is large compared to the roughness of the contacting surfaces. Load passing gives a two dimensional profile with shear stress varying with depth and compressive direct stress varying with width. These stresses are not proportional to time so, in this respect, even the simplest RCF differs from classical fatigue. The situation is more complex in realistic conditions where roughness is appreciable and tractive or sliding forces are involved, so during RCF, the stresses are local, compressive, non-proportional to time and randomly fluctuating in direction and magnitude. Plastic deformation often precedes crack formation on the scale of either the Hertz contact or the roughness. This happens on softer or tougher materials and gives rise to an accumulation of plastic strain (ratcheting) under elastic and plastic shakedown loads (Figure 1.3). In hard materials, RCF is less commonly accompanied with plasticity. Here, crack initiation occurs at surface asperities, dents or subsurface inclusions.

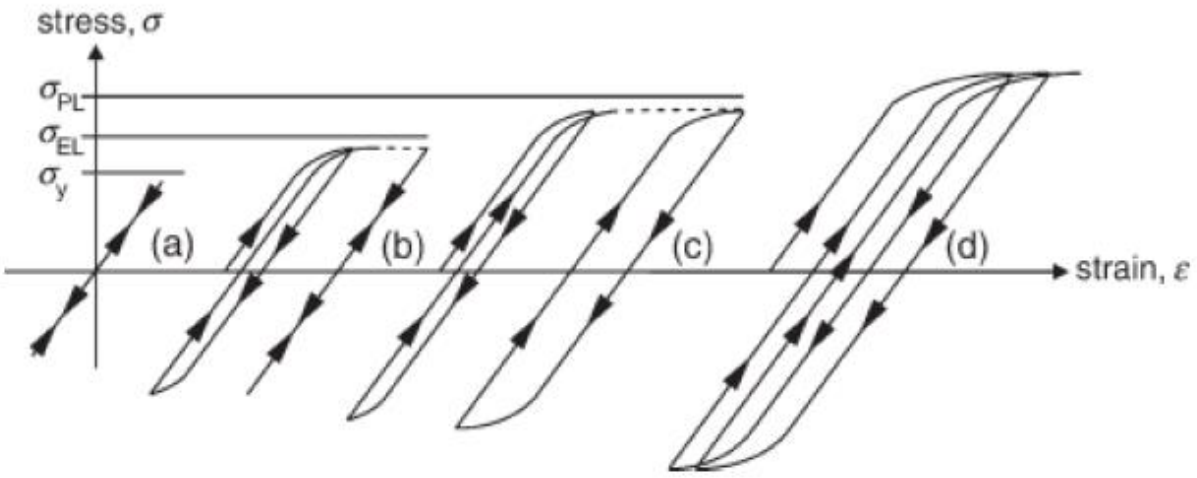

Figure 1.3: Material response to cyclic loading (a) perfectly elastic (b) elastic shakedown

(c) Plastic shakedown and (d) ratcheting [21].

Further, due to stain localization, compressive stresses become extensive at crack closure and RCF develops due to crack face friction and interlocking that initially causes crack development, which is mechanically influenced by lubrication near the crack face (Figure 1.4).

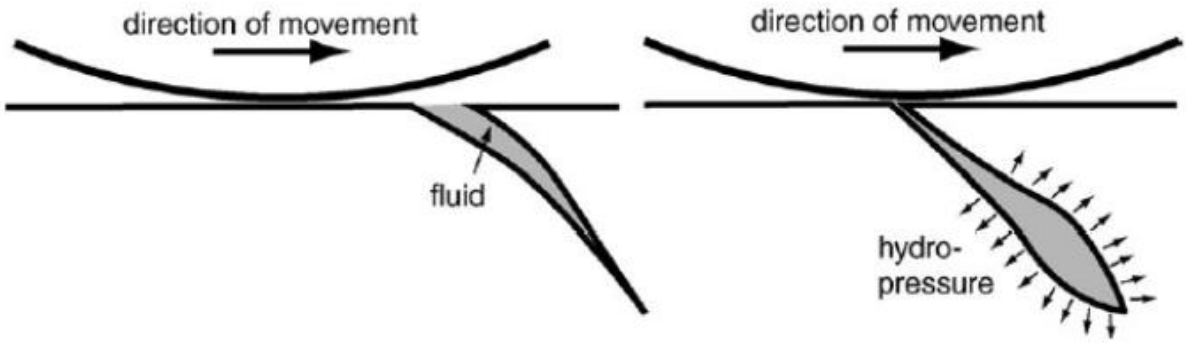

Figure 1.4: Crack propagation mechanism by pressure of trapped fluid [18].

1.2. Problem statement

While many parts may work well initially, they often fail in service due to fatigue failure caused by repeated cyclic loading. In practice, loads significantly below static limits can cause failure if the load is repeated sufficient times. Thus, Wheel-rail rolling contact is subjected to repeated mechanical cyclic stress/strain, and causes in sever damages. Wheel-rail interface is the vital component at which the vehicle interacts with the track. Wheel-rail contact is subjected to a series of normal and tangential forces due to the weight, curving and tractive effort. Most of wheel-rail contact failures are caused by rolling contact fatigue. Thus, wheel-rail contact needs to have an excellent fatigue life. Characterizing the capability of a material to survive the many cycles a component may experience during its life time is the aim of fatigue analysis. Thus, this thesis intends to predict the fatigue life at the wheel-rail rolling contact using finite element method (FEM) ANSYS software. Prediction, identification and treatment of wheel-rail rolling contact fatigue (RCF) is essential for ensuring safety, increasing wheel/rail life and reducing maintenance and costs. This study is based on AA LRT real conditions and specifications.

1.3. Objective of the thesis

1.3.1. General objective:

- The general objective of the study is to analyze the rolling contact fatigue at the wheel-rail interface using FEM ANSYS software.

1.3.2. Specific objective:

- To predict fatigue life at the wheel-rail rolling contact using 3D finite element analysis ANSYS software based on the stress fatigue analysis.
- To determine the stresses and strains induced at the wheel- rail rolling contact at different sections of the track; namely straight, transition curve and circular curve track.
- To investigate the effect of rolling contact coefficient of friction and track conditions (at straight, transition and circular curve track paths) on the rolling contact fatigue at the wheel-rail interface.

1.4. Scope of the thesis

This thesis covers analysis of rolling contact fatigue at wheel-rail interface. The rolling contact fatigue failure is assumed due to the mechanical loads only. Track conditions (straight, transition curve and circular curve track) and rolling contact coefficient of frictions (0.15, 0.3, 0.6) are taken for this investigations. For the fatigue analysis 3D finite element method ANSYS software is used. The vertical load, lateral load and rotational effect of the wheel are considered during the FEA. The fatigue analysis is based on the stress life.

1.5. Significant of the study

The thesis is very valuable for fatigue resistance design and inspection planning for wheel and rail for light rail transit (AA LRT) in Ethiopia.

1.6. Research methodology

To achieve the scope of the thesis the following methodological approaches are performed.

1.6.1. Data collection:

Necessaries data and specifications are gathered from AA LRT project office. And also different articles, journals, and other related documents are used to perform the thesis work.

1.6.2. Data analysis:

First, analytical analysis is performed to obtain the input loads for the FEA. And then FEA is performed in ANSYS software. Wheel and rail geometry assembly model is created in CATIA software, then the assembled part is imported to ANSYS workbench and Necessary engineering data or material mechanical properties are inserted. Next finite element modelling is performed. Meshing and contact sizing is performed, and boundary conditions and loadings are applied. Finally the FEA (fatigue analysis) is done after all necessary parameters are selected.

1.6.3. Result presentation:

For easily readable and clearly understandable for readers, the obtained results are presented in tables, graphs and plots form.

1.7. Thesis layout:

The thesis focuses on the analysis of rolling contact fatigue at the wheel-rail contact. And it has six parts (chapters). The first chapter is the introduction part which clearly describes the general background of the study, statement of the problem, and objective, scope of the study, and research methodology, the second chapter describes related literature reviews about the thesis topic; analysis of rolling contact fatigue at the wheel-rail interface. These literature reviews are basics for the present thesis, the third chapter contains the collected data and specifications and the analysis of forces at different track conditions (at straight, transition curve, and circular curved track paths). The aim of this chapter is to obtain the input contact forces for the FEA (fatigue analysis), the fourth chapter is the main body of the thesis. It includes the material mechanical properties, geometry modelling, and finite element modeling and FEA (fatigue analysis) and the next chapter presents results and discussions. In this chapter the simulated model gives results in counter plots and the obtained results are discussed one by one in tables and graphs form and the last chapter describes briefly the conclusion, recommendations, and future works of the thesis. The overall results and scopes of the thesis are described in the conclusion part. Based on the FEA results, Suggestions and recommendations are given and finally the continuity of the paper or future works are mentioned.

CHAPTER TWO

LITERATURE REVIEWS

[35] Conducted on Fatigue crack initiation life prediction of railroad wheels. In the paper a new multiaxial high-cycle fatigue initiation life prediction model for railroad wheels is proposed. A general fatigue damage analysis methodology for complex mechanical components is developed and applied to the wheel/rail rolling contact fatigue problem. A 3-D elasto-plastic finite element model is used for stress analysis. A sub modeling technique is used to achieve both computational efficiency and accuracy. All the finite element models are built using the commercial software Ansys7.0. Then the fatigue damage in the wheel is evaluated numerically using the stress history during one revolution of the wheel rotation. The effects of wheel diameter, vertical loading, material hardness, and material fatigue properties on fatigue crack initiation life are investigated using the proposed model. [36] Studied on wheel-rail contact fatigue. The study focused on initiation of wear and crack and modelled wear, crack ignition and combination of the two. The mechanism for surface layer wear is crack propagation. The surface rapidly exhibit Micro cracking. Micrograph of the contacting surface and wear debris for twin disc tests and rail have shown that wear proceeds by removal of flakes from the surface. Some twin disc tests have shown that even in dry contact, RCF (Rolling Contact Fatigue) cracks could eventually initiated. However with a fluid present, the micro cracks typically propagate further into the rail and produce RCF defects. There are two mechanism by which the presence of fluid can promote crack growth instead of wear. These are alteration to the friction between the cracks faces, allowing them to slide over each other easier and hydraulic pressurization on the crack faces. Due to pressure involved, cracks are more likely to grow under the opening hydraulic loading if they are sufficiently well sealed for pressure to apply load to the crack faces before the fluid escapes. However, finite element modeling has shown that, at normal operating speeds, a crack opening is too rapid for water to be drawn in to the cracks, suggesting that unless water is already present by capillary action during it into the crack, hydraulic pressure could not be generated. Conversely, if there were fluid in the crack prior to passing contact, it would not have sufficient time to flow out. Thus, friction alteration combined with pressurization of fluid already in the crack is likely to be the cause of increased crack growth. As a simulation is conducted rolling/sliding contact loads are applied to the rail by

passing wheels. [37] Studied on Design and Analysis of Train Wheel during Rolling Action. This paper gives, a detailed overview of the rolling contact problem of train wheels was given by different failure modes have been observed for train wheels in rim damage, train suspensions. The rolling contact of a wheel on a rail is the basis of many Rail-Wheel related problems including the rail corrugation, wear, and plastic deformation, rotating interaction fatigue, thermo-elastic-plastic-behavior in contact, fracture, creep, and vehicle dynamics vibration. The modelling tool and a methodology are described in this presented paper. Simulation results are compared with Hertz a solution for stress calculations. ANSYS software is utilized with the purpose of simulating the system. Three different procedures have conventionally been utilized to inspect Rail-Wheel contacts including Hertz's analytical method, Walker's programs, and contact and fasts. The calculation of these stresses becomes much more complicated in three dimensional real size geometries. Thermal cracking usually breaks off a piece of the wheel tread, while shattered rim can destroy the wheels integrity, and is thus more dangerous. Shattered rim failures are the result of large subsurface cracks that propagate roughly parallel to the wheel tread surface. The contribution of this research is to establish a widely known FEM on a 3D Rail-Wheel. Fatigue crack initiation model, Bernasconiet all examined several multi axial fatigue models by using Hertz contact theory for the wheel material. Guo and Barkey used a 2D finite element model and a multi axial fatigue model developed by Fatemi and Socie for rolling contact fatigue analysis. Sraml et al. use the Hertz theory to calculate the stress response and treat the multi axial fatigue problem as a fatigue problem. The principal stress/strain component in one direction is used for fatigue analysis, which uses 3D finite element analysis but applied the contact pressure based on Hertz theory. A developed fatigue life prediction methodology for the wheel/rail contact fatigue problem, which uses the Hertz contact theory for stress calculation and multi axial fatigue model proposed. [38] developed three-dimensional elastic-plastic finite element analysis for wheel-rail rolling contact fatigue. In this paper, three-dimensional elastic–plastic stress analysis of rolling contact of railway wheel is conducted on a 3D wheel-rail model. Then, the contact pressure distributions calculated using elastic Hertz theory and three-dimensional elastic–plastic stress analysis are compared. Finally, the FEM results are analyzed adopting Dang Van criterion [40] for RCF life assessment of the railway wheels. [46] Investigated the effects of axle load and train speed at rail joint using finite element method. The goal of this research was to investigate the effects of axle load and train speed at rail joint. A three-dimensional finite element analysis of a

rail/wheel contact is conducted on the rail joint section of track and dynamic load is applied to develop an estimate respective stresses at the section. The finite element program ANSYS is used to model the contact analysis. The ANSYS is used to simulate the loading and boundary conditions of the rail and wheel contact for a stress analysis. Material properties are assumed to be same for rail and wheel, and considered to be bilinear kinematic hardening in ANSYS.A 3-D finite element model for element model for wheel/rail rolling contact is developed on the most critical section of rail track i.e., rail joint to calculate elastic-plastic finite element analysis and 3D stress response in the contact region. These models should be accurately calculating the 3D stress response in the contact region. The reason for this study was to investigate possible changes in rail and wheel contact design in order to improve the performance of the rail track. Obtained results indicated that the von mises stresses, the maximum shear stress and the Equivalent elastic strain are increases linearly with increasing axle load and the effect of train speed on above parameters is relatively weak. [39] developed an Analysis of Rolling Contact Fatigue Damage Initiation in Wheel-Rail Interface. The paper presented the analysis of RCF damage initiation and stress distribution at the wheel-rail interface at different directions. A three-dimensional elastic frictional finite element model of the wheel-rail interaction is used to investigate the effect of the applied contact loading force at the straight, transition, and curved areas of the wheel tread and railhead surface. The interaction between the left and right wheels is considered. The interface exhibits small damage problems that are solved via the finite element method (FEM) software code ANSYS 11. The half-space assumption of the Hertz method is avoided by FEM. The real geometry and the boundary condition of the wheel-rail interface are accurately shown by the proposed simulation. The simulation is a set of the element size and the quasi-static loads on the wheel created with a library of ANSYS 11. Force is applied on the wheel which has contact with the rail. Here, the rail and the wheel tread are defined as two separate profiles. The Goodman approach in ANSYS 11 via the FEM is used in all simulations to predict the mean stress effects.

The present thesis presents analysis of rolling contact fatigue at wheel-rail contact based on Addis Ababa light rail transit (AA LRT) real conditions and specifications. The aim of the thesis is to predict the fatigue life at the wheel-rail rolling contact at different track conditions, (at straight, transition and circular curve track) and to investigate the effect of rolling contact coefficient of friction on the fatigue life at the wheel-rail rolling contact using FEM ANSYS software.

CHAPTER THREE

DATA COLLECTION AND CONTACT FORCE ANALYSIS

3.1. Data collection

3.1.1. General AA LRT track conditions

Table 3.1 AA LRT track conditions [50]

Track gauge	1435mm
Rail cant	1in 40
Minimum radius of horizontal curve	50m
Maximum superelevation of curve	120mm
Type of rail	50 Kg/m

3.1.2. General AA LRT vehicle specifications

Vehicles are 70% low floor modern trams with maximum operating speed of 70km/h, and Average travelling speed ≥ 20km/h. The wheel rolling diameter is 660mm [51]. The total vehicle weight is described in table 3.2.

Table 3.2: AA LR vehicle weight specifications [51]

Loads	Car body weight	Passenger weight	Total weight
Empty vehicle (t)	44	0	44
Rated passenger capacity (t)	44	15.24	59.24
Overload capacity (t)	44	19.02	63.02
Axle load(t)	≤ 11(1+3%)t		

Note: Take 60kg as average weight of each passenger [51]

3.2. Force analysis for single wheelset

3.2.1. Normal contact forces on straight track path

For an applied load on a wheel-rail interface, normal contact forces develop on the contact patch depending on the total vertical force applied and the contact angle of the wheel-rail contact formed as a result of the lateral displacement, y of the wheelset during motion [41]. However, on the tread with a low conicity the normal load, F_N has practically the same value as the vertical load on the wheel. Therefore, for this thesis for small lateral displacement, the normal contact forces, F_{NLw} and F_{NRw} on the left and right wheels respectively are assumed to be the same.

$$F_{NLw} = F_{NRw} = \frac{W}{2} = \frac{mg}{2} \tag{3.1}$$

Thus, $F_{NRw} = \frac{11330*9.81}{2} = 55573.65N$

Where,

W is axle weight (the product of axle load, m and gravitational acceleration, g)

m is axle load, 11(1+3%)t = 11330Kg

g is gravitational acceleration constant = 9.81m/s^2

3.2.2. Kinematic Analysis of the Wheelset on Curved Track

3.2.2.1. *Wheelset geometry and the role of the wheel conicity*

In curving situations, the conicity of the wheel treads serves a similar function to the differential in an automobile [42]. In an automobile, the differential is necessary when the vehicle turns, because it allows the driving road wheels to rotate at different speeds. This allows the wheel on the outside of turning curve to roll faster (at a higher angular velocity) than the other, allowing it to traverse the greater distance. Unlike in an automobile, whose differential allows the wheels to spin at different speeds, in a railcar the two wheels are fixed to a common axle and therefore must rotate at the same speed. In this case, it is the conicity that allows the wheel on the outside of the turn to move faster and cover the longer distance. On a gentle curve, the coned wheels maintain pure rolling motion by moving laterally outward and adopting a radial position. In this way, the wheel on the outside of the curve runs on a larger radius (and therefore circumference) and can

travel the greater distance at the common angular speed; whereas the wheel on the inside of the curve rolls on its smaller radius and travels the smaller distance. So a rigid wheelset with coned wheels maintains pure rolling motion in a gentle curve, without flange contact, if it moves laterally outward a distance, y from the center of the track and adopts a radial position as shown in fig. 3.1.

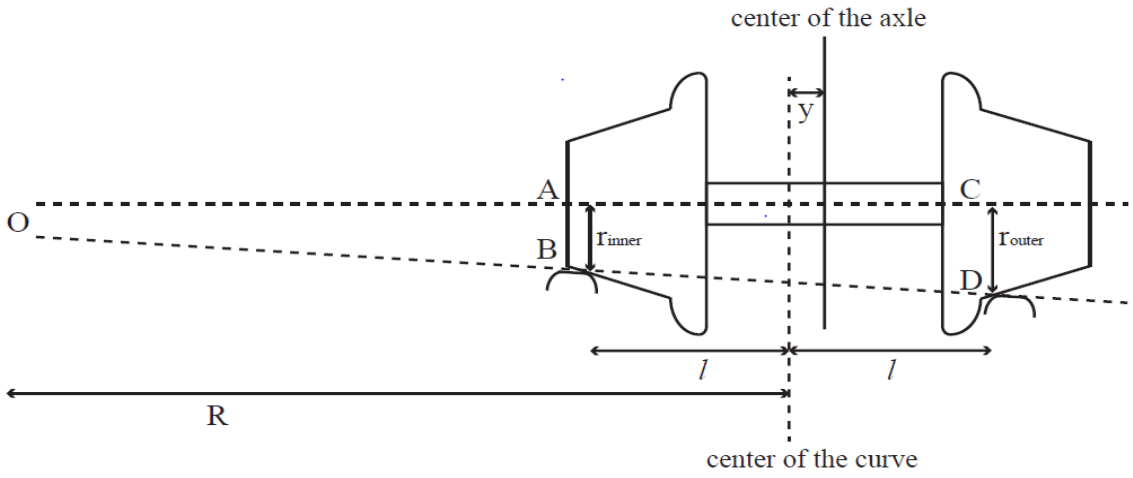

Figure 3.1: Geometry of a coned wheelset on a gentle curve [41].

We construct two rays from the origin of the curve, O. The first passes through the contact point of the inner wheel and rail, B, and the contact point of the outer wheel and rail, D. The second ray lies along the central axle axis, connecting the origin of the curve with the center of the inner wheel, A and the center of the outer wheel, C. These two rays form an angle at the center of the curve and give rise to similar triangles AOB and COD. Using properties of similar triangles, we can write the relation [41]:

$$\frac{r_{inner}}{R-l} = \frac{r_{outer}}{R+l} \tag{3.2}$$

Where, R is the radius of the curve, 2l is the contact distance (the lateral distance between the points of contact of the wheels with the rails), r_{inner} is the radius of the wheel on the inside of the curve at the point of contact with the rail and r_{outer} is similarly the radius of the wheel on the outside of the curve at the point of contact with the rail. If we define the normal running radius, r to be the radius of both wheels when the wheelset is centered on the track, then we can rewrite r_{inner} and r_{outer} in terms of the conicity of the wheelset, δ and the lateral displacement of the wheelset, y.

$$r_{inner} = (r - \delta y) \tag{3.3}$$

$$r_{outer} = (r + \delta y) \tag{3.4}$$

By substituting these expressions for r_{inner} and r_{outer} into the similar triangles relation, we can solve for the lateral displacement, y in terms of physical parameters of the wheel rail system, the tread conicity, δ normal wheel radius, r track gauge plus rail head width (distance between wheelset contacts), 2l and radius of curvature, R:

$$y = \frac{rl}{R\delta} \tag{3.5}$$

3.2.2.2. *Curving and the Role of the wheel Flange*

When a body accelerates, or changes velocity, that acceleration is accompanied by a force according to the equation F = m*a [41], where the mass of the object, m is its weight, W divided by the gravitational acceleration constant, g. We tend to think of acceleration as being a change in speed; but since velocity is a vector, any change of velocity be it a change in the magnitude (speed) or in the direction requires a force. For instance, in circular motion at constant speed, there is an acceleration radially inward toward the center of rotation due to the changing direction of the tangential velocity. It is this centripetal acceleration (and accompanying force) that keeps the object moving in a circular path. However, the objects inertia resists this change and so always acts in the opposite direction of the acceleration, or in this case radially outward from the center of the circle. For a railcar and attached wheelset going around a curve, it is the train's inertia that causes instability and guidance problems such as tipping or derailment. In stable curving, lateral forces between the wheels and the rail provide a centripetal acceleration equal to the square tangential velocity of the train down the track, V^2 divided by the radius of the curve, R.

$$a_c = \frac{V^2}{R} \tag{3.6}$$

The centripetal force associated with this acceleration keeps the train in a circular, or curved path; however, the train's inertia acts in the opposite direction of this acceleration. Since the resistance from inertia has the same units as a force, it is commonly (and erroneously) referred to as the centrifugal force. Often these 'fictitious forces' arise from a difference in reference frames. From the viewpoint or reference frame of someone on the ground beside the track, there appears to be no force acting outward on the railcar. However, from the rotating reference frame of the railcar

itself, the car's inertia resists the circular motion and the railcar experiences a push or pull similar to a force. In other words, the centrifugal force is simply the train's inertial resistance to the centripetal acceleration around a curve and can be calculated using F = m*a. For a locomotive traveling at a forward speed, V on a flat curve of radius, R the centrifugal inertial loading is given by:

$$F_c = m * a_c = m * \frac{V^2}{R} \tag{3.7}$$

Where,

m is axle mass

a_c is centrifugal acceleration

V is speed of the vehicle

R is track curve radius

Based on this formula the centrifugal force for single wheelset at the minimum track curve radius, R=50m, is given as:

$$F_c = m\frac{V^2}{R} = 11330 * \frac{19.44^2}{50} = 85635.22N$$

Lateral forces between the wheels and the rail must react against the centrifugal inertial loading to keep the train on the tracks. If the centrifugal inertial loading is excessive, the locomotive begins to tip. The flange of the wheel catches on the rail and the locomotive starts to rotate. In fact, this is why the flanges are on the inside of the wheels. In sharp curves, if the flange is on the inside, then the lateral force applied by the rail to the leading wheelset is applied to the outer wheel and will be combined with an enhanced vertical load, diminishing the risk of derailment. If the flanges were instead on the outside, the slightest bit of wheel lift would slide the locomotive off the tracks.

3.2.2.3. *Contact forces during curve negotiation with flange contact on the right wheel*

The 1947 accident occurred on a flat curve, at a time when old infrastructure had yet to be upgraded to allow for faster speeds and higher traffic flows. In modern industrial practice, many tracks are designed so that rails are not flat on curves. Instead, the curve is banked so that the outside rail on a curve is elevated higher than the inside rail. This superelevation (or cross level in the US) is usually characterized by the height difference between the tops of the rails, but can also be measured in terms of angle or cant. The relationship between the cant angle and superelevation height, s is dictated by the rail contact distance according to simple right-triangle geometry.

$$sin\varphi = \frac{S}{2l} = \frac{120mm}{1505mm} = 0.0797342 \tag{3.8}$$

Where, the maximum superelevation is, S = 120mm, and track gauge plus rail head width (i.e. distance between contacts) is, 2l = 1505mm.

Therefore, **φ = 4.573º**.

A raised outside rail rotates the train toward the inside of the curve and helps fight off the overturning rotation toward the outside of the curve caused by the centrifugal inertial loading.

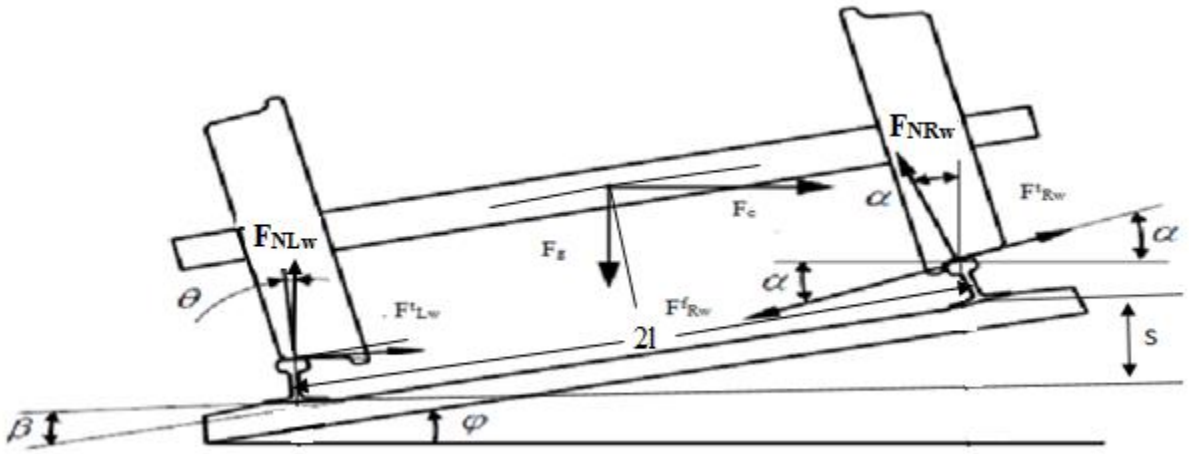

Figure 3.2: Wheelset forces during curve negotiation with flange contact on the right wheel [43].

In Figure 3.2 are represented the forces acting on the wheelset when it travels in the circular curve and flange contact occurs on the right wheel. The quantities, F_{NLw} and, F_{NRw} represent the normal contact forces on the left and right wheels, respectively. F^t_{Lw} and, F^t_{Rw} are the lateral contact forces

on the treads of the wheels, F^f_{Rw} is the lateral flange force on the right wheel, and, F_g and F_c are the gravitational and the centrifugal forces acting on the wheelset. The angle, φ represents the track cant angle, β is the rail inclination angle, and θ and α are the angles associated to the sets of forces acting on the left and right wheels, respectively.

An equilibrium of forces in the vertical and horizontal directions can be written in the form:

Vertical forces:

$$\sum F_y = 0$$

$$F_{NRw}cos\alpha + F_{NLw}cos\theta + F^t_{Rw}sin\alpha - F^f_{Rw}sin\alpha - F^t_{Lw}sin\theta - F_g = 0 \quad (3.9)$$

$$\therefore F_g = F_{NRw}cos\alpha + F_{NLw}cos\theta + F^t_{Rw}sin\alpha - F^f_{Rw}sin\alpha - F^t_{Lw}sin\theta \quad (3.10)$$

Lateral forces:

$$\sum F_x = 0$$

$$-F_{NRw}sin\alpha + F_{NLw}sin\theta - F^f_{Rw}cos\alpha + F^t_{Rw}cos\alpha + F^t_{Lw}cos\theta + F_c = 0 \quad (3.11)$$

$$\therefore F_c = F_{NRw}sin\alpha - F_{NLw}sin\theta + F^f_{Rw}cos\alpha - F^t_{Rw}cos\alpha - F^t_{Lw}cos\theta \quad (3.12)$$

Where,

$$F_g = W = mg = 11330 * 9.81 = 111147.3N$$

$$F_c = m * \frac{V^2}{R} = 11330 * \frac{19.44^2}{50} = 85635.22N$$

$$F^t_{Lw}, F^f_{Rw}, F^t_{Rw} = \mu F_N$$

$$\alpha = (\varphi + \beta) = 6.005^o$$

$$\theta = (\varphi - \beta) = 3.141^o$$

β is 1.432° and φ is 4.573°.

W is axle weight (mg)

V is vehicle speed (19.44m/s)

R is radius of curvature (50m)

F_N is normal force

μ is coefficient of friction. For this analysis, assume the rolling coefficient of friction, μ at wheel-rail contact is 0.3.

Therefore, by solving eqn. (3.10) and (3.12) simultaneously, we can obtain the normal loads at the right wheel, i.e. F_{NRw} = **271332.15N**.

Now the vertical force applied at the outer wheel (at the right wheel) is given as;

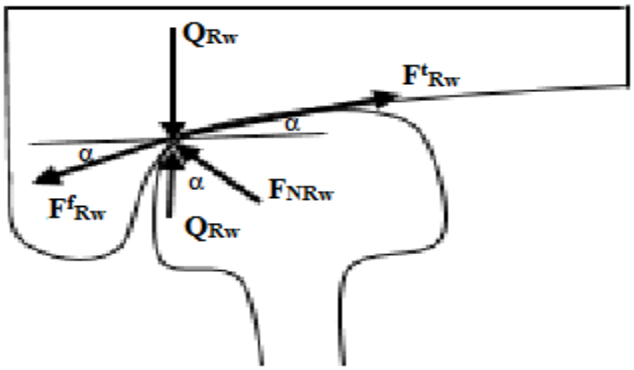

Fig.3.3. Vertical force on the outer right wheel.

$$Q_{Rw} = F_{NRw}cos\alpha = 271332.15 * \cos(6.005) = 269843.28N$$

3.2.2.4. *Contact forces at the transition curve track*

Transition curves are curves in which the radius gradually changes from infinity to a particular value R. The effect of this is to gradually increase the radial force for, F_c from zero to its maximum value, thereby reducing its effect. To introduce, F_c uniformly along the length of the transition curve, F_c must also be proportional to the length of the transition curve, L. A curve is necessary to smoothly change the direction of a moving vehicle. However, as the vehicle enters or leaves a curve (a Simple Circular Curve) sudden change of direction implies sudden change of radial acceleration, $\frac{V^2}{R}$ causing inconveniences to the passengers. This can be avoided by introducing a special curve called a Transition Curve between the straight section (initial section) and the beginning of circular curve followed by another transition curve between the final section and the end of circular curve as shown in Fig.3.3.

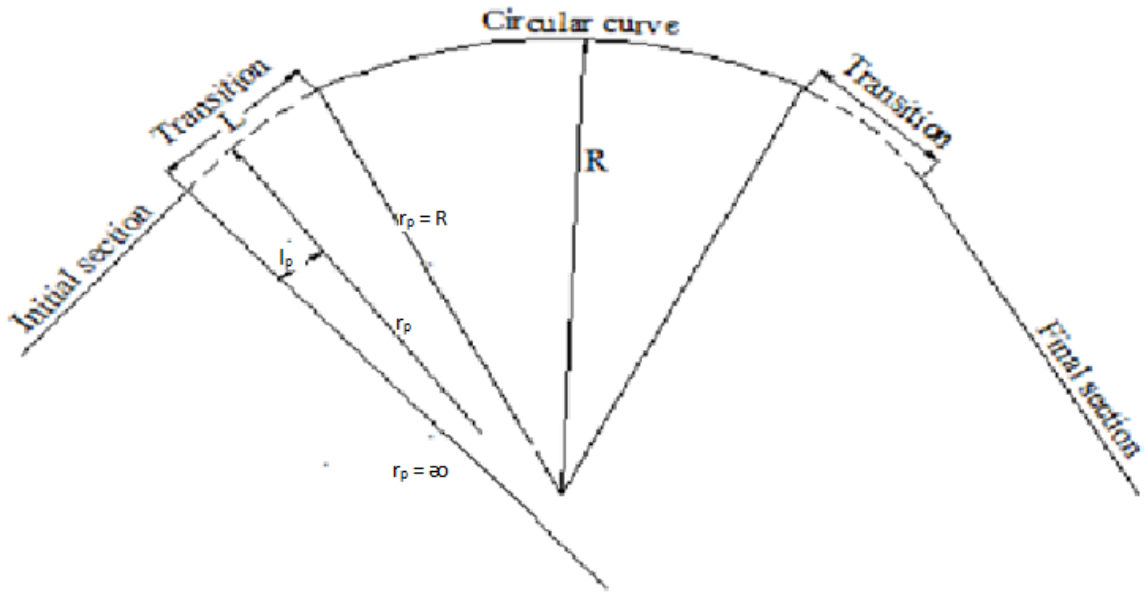

Fig.3.4. Formation of transition curves between straight and circular sections [44].

Note that the centrifugal force, F_c at any point on the transition curve is proportional to the distance of that point from the starting point of the curve.

Therefore, at constant mass and design speed, the radial force, F_c is given by:

$$F_c \propto l_p \propto \frac{1}{r_p} \tag{3.13}$$

From this relation,

$$l_p \propto \frac{1}{r_p} \quad i.e.\ l_p r_p = K\ (a\ constant) \tag{3.14}$$

Therefore, for each transition in a transition curve the radius R and length L can be designed to equal to K over the whole length of the curve [44].

$$\text{At, } l_p = L, and\ r_p = R,\ RL = K \tag{3.15}$$

$$\therefore l_p r_p = LR = K \tag{3.16}$$

$$r_p = \frac{LR}{l_p} \tag{3.17}$$

Where,

l_p is length of transition curve at any point

L is total length of the transition curve

r_p is radius of transition curve at any point

R is radius of circular curve

Thus, according to AA LR track design the minimum horizontal curve radius which is found at Meskel Square (the track that comes from kaliti turns to stadium or mexico) is selected for this study. Based on this design the curve radius, R is 50m and the transition length, L is 20m. for this analysis assume, l_p is 1/20 of the length of the total transition curve length, L = 20m. Therefore, l_p will be 1m and then r_p will be 1000m.

Then, at rp = 1000m of the transition curve length, the centrifugal force is given as:

$$F_c = m\frac{v^2}{r_p} \tag{3.17}$$

$$F_c = 11330 * \frac{19.44^2}{1000} = 4281.76N$$

Where,

m is axle load

V is design vehicle speed.

rp is radius of curve at any point of the transition curve length.

Here, the superelevation height, s or track cant anngle, φ at the transition curve is inversely propertional to r_p. since, r_p varies linearly with l_p, so can cant. Therefore, the superelevation angle or track cant angle, φ from fig.3.5 is obtained from the relation as below:

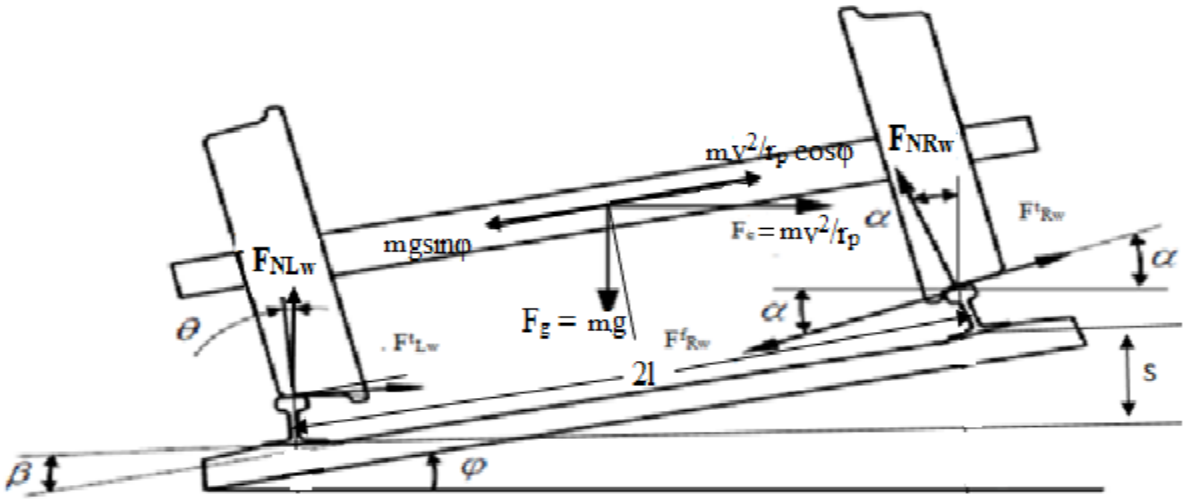

Figure 3.5: Forces acting on a vehicle at a transition curve on superelevated track.

$$m\frac{v^2}{r_p}cos\varphi = mgsin\varphi \tag{3.18}$$

$i.e.tan\varphi = m\frac{v^2}{r_p} \div mg = \frac{v^2}{r_p g}$, it is also known as centripetal ratio.

$$\therefore tan\varphi = \frac{19.44^2}{1000*9.81} = 0.038523$$

$$\varphi = 2.206\ ^{o}$$

Known,

$\alpha = \varphi + \beta = 2.206 + 1.432 = 3.638^{o}$.

$\theta = \varphi - \beta = 2.206 - 1.432 = 0.774 \sim 0$

$s = 2l * tan\varphi = 1505 * \tan(2.206) = 57.974mm$

Therefore, from eqn. (3.10) and (3.12);

$$F_g = F_{NRw}cos\alpha + F_{NLw}cos\theta + F^t_{Rw}sin\alpha - F^f_{Rw}sin\alpha - F^t_{Lw}sin\theta \tag{3.18}$$

$$F_c = F_{NRw}sin\alpha - F_{NLw}sin\theta + F^f_{Rw}cos\alpha - F^t_{Rw}cos\alpha - F^t_{Lw}cos\theta \tag{3.19}$$

Known,

$$F_g = W = m * g = 111147.3N$$

$$F_c = m * \frac{V^2}{r_p} = 11330 * \frac{19.44^2}{1000} = 4281.76N$$

By subsitituting, these values to eqn. (3.18) and (3.19) and solving simultaneusly to get the normal contact forces at the outer wheel.

Therefore, **F_{NRw} will be 103709.89N,** and then the vertical force at the right wheel, **Q_{Rw} will be 103500.9N.**

CHAPTER FOUR

FINITE ELEMENT MODELLING AND ANALYSIS

4.1. Wheel and rail material properties

Rail material should be selected based on an integrated consideration of lines conditions, operation load situation, the matching with wheel hardness, rail load and wear resistance, and maintenance and repair. The rail for AA LRT is based on Chinese specification 50Kg/m. Rail material generally used in domestic urban rail transit are U71Mn and U75V [50]. The U71Mn rail, with its tensile strength and yield strength being not less than 880Mpa and 457Mpa respectively, and the U75V rail, with its tensile strength and yield strength being not less than 980Mpa and 880Mpa respectively.

However, the U71Mn rail should enjoy priority in the whole line construction, considering the functional requirements of use [50]. Therefore, for this finite element analysis (FEA), the mechanical material properties of the wheel and rail are assumed to be the same and listed in table 4.1.

Table 4.1. Mechanical material properties of wheel and rail steel [46].

Material properties	values
Poison ratio	0.3
Young's modulus	210Gpa
Material density	7820 Kg/m
Yield strength	500Mpa
Tangent modulus	4000Mpa
Ultimate tensile strength	880Mpa
Tensile yield strength	540Mpa
Compressive yield strength	540Mpa

4.2. Wheel-rail assembly geometry model

The wheel and rail is based on AA LRT specifications. The wheel has a rolling diameter 660mm, and its profile is based on UIC60, and the rail is based on UIC50 profile. Thus, the radius of curvature of the rail head is 300mm. For this model a piecewise rail is taken with length of 600mm that is the average distance between two sleepers. The wheel and rail are created separately and then assembled in CATIA software as in fig.4.1.

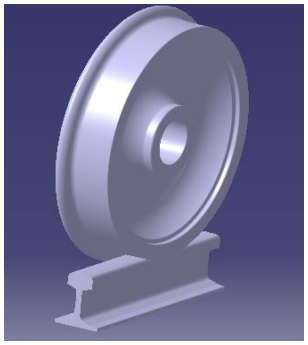

Figure 4.1: Wheel-rail assembly geometry model in CATIA software.

4.3. Finite element (FE) model

To perform the objective and scope of the thesis, a 3D elasto-plastic finite element model is used. All the finite element models are built using ANSYS software. The general procedure is first, the 3D geometry model is transferred or imported to ANSYS software and then meshed with ansys workbench. The meshing at the contact location is refined very well for efficient and accurate computation as shown in Fig. 4.2, fig. 4.3 and Fig. 4.4. The contact between rail and wheel is modeled using ANSYS workbench. The total vertical load of 11(1+3%)t per axle is applied. Wheels are assumed to operate on a straight, transition and circular curve track path. Therefore, lateral loads to the system are considered and the rotational effect of the wheels is also considered. The coefficient of friction at the wheel-rail rolling contact varies according to the track and environmental conditions. Based on these conditions the rolling contact friction coefficient, μ= 0.15, 0.3 and 0.6 is used in the FE analysis for this investigation. The rail and wheel material properties are assumed to be the same, and a bilinear kinematic hardening elastic–plastic material model is used in ANSYS workbench. Boundary and loading conditions are applied to the model. The rail is fixed at both ends and bottom of the rail to prevent rigid body motion of the whole

system. The mounting slope of the rail on the ground (1/40 radian) is taken into consideration for contact analysis of wheel-rail contact.

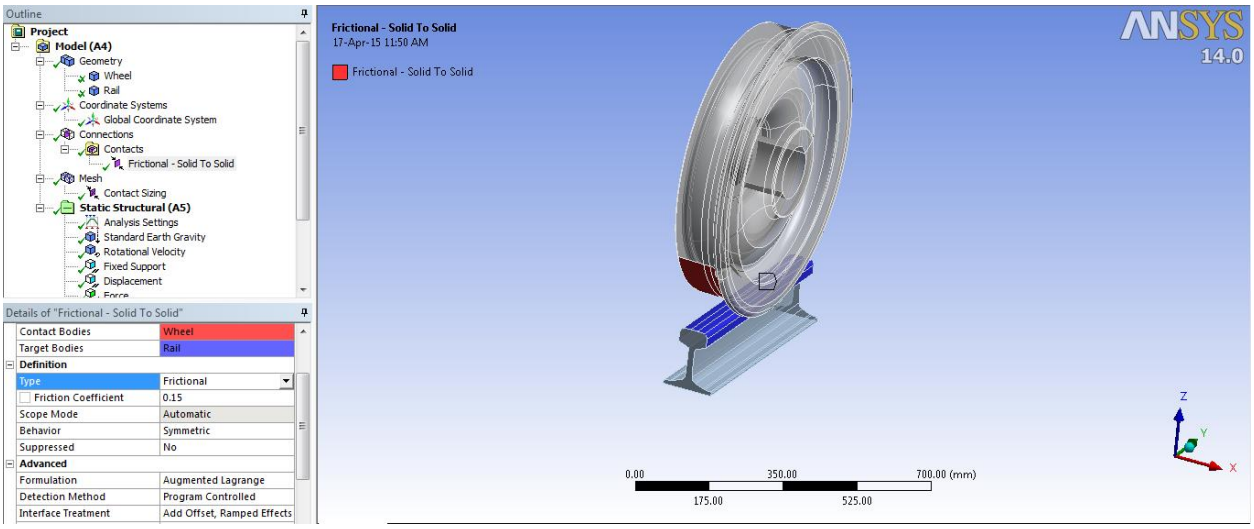

Figure 4.2: Wheel-rail contact modelling in ANSYS workbench

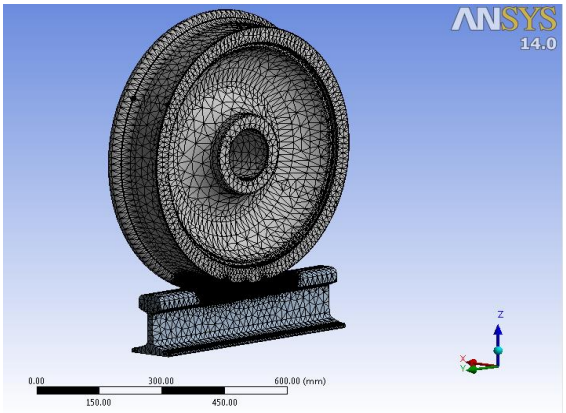

Figure 4.3: Finite element model meshing and contact sizing with rail head center and wheel tread center in contact at straight track path. (number of nodes: 341056 and number of elements: 199293)

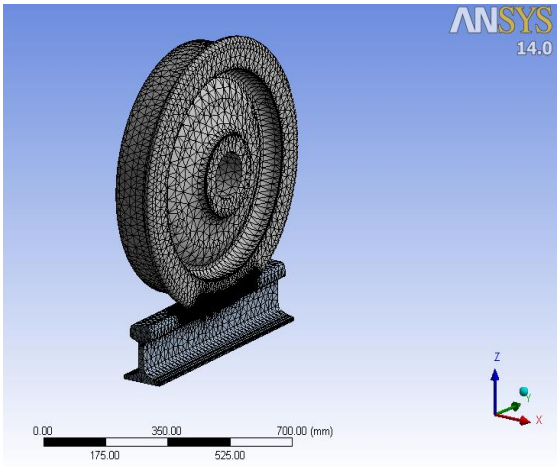

Figure 4.4: Finite element model meshing and contact sizing at the wheel-rail contact at transition curve track path. (number of nodes: 395122 and number of elements: 231112)

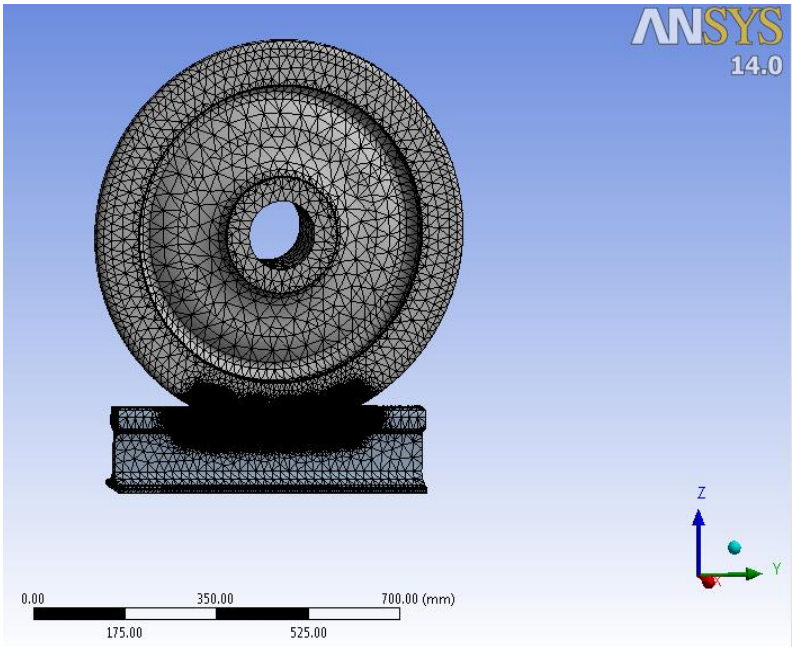

Figure 4.5: Finite element model meshing and contact sizing with flange contact at the circular curve track path. (number of nodes:471738 and number of elements:276966).

4.4. Loading and boundary conditions

The geometrical boundary conditions and loadings are applied based on physical characters and real conditions of the AA LRT. For this finite element analysis, we consider the outer wheel only. The train speed, V is 70 km/h or 19.44 m/s or 58.9 rad/sec, and the vertical contact forces are, 55573.65N, 103500.9N, 269843.28N on straight, transition curve, and circular curve track path respectively. The lateral forces are 4281.76N, and 85635.22N on the transition and circular curve track path respectively. 50Kg/m rail is used and the length of the rail is the average distance between two slippers i.e. 600mm, and the rail is fixed at both ends and bottom of the rail; because the rails at the elevated track (around Meskel Adebabay) are supported or fixed wholly on concrete. The diameter of wheel is 660 mm. The wheel is constrained to both directions (longitudinally and laterally). All the loads are applied at the center or hub of the wheel. The mechanical material properties are assumed to be the same for both rail and wheel and considered to be bilinear kinematic hardening in ANSYS.

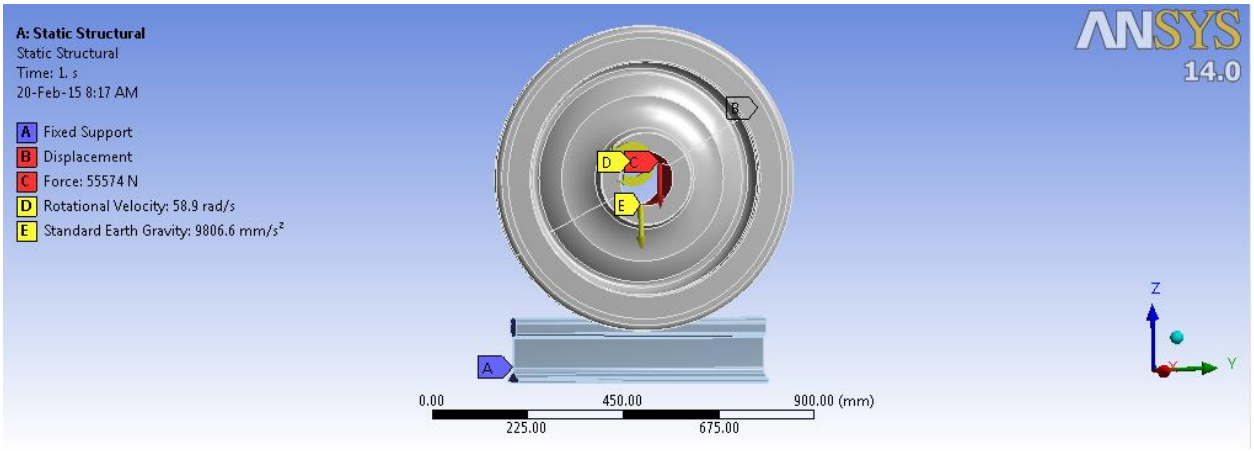

Figure 4.6: Loading and boundary conditions at straight track path.

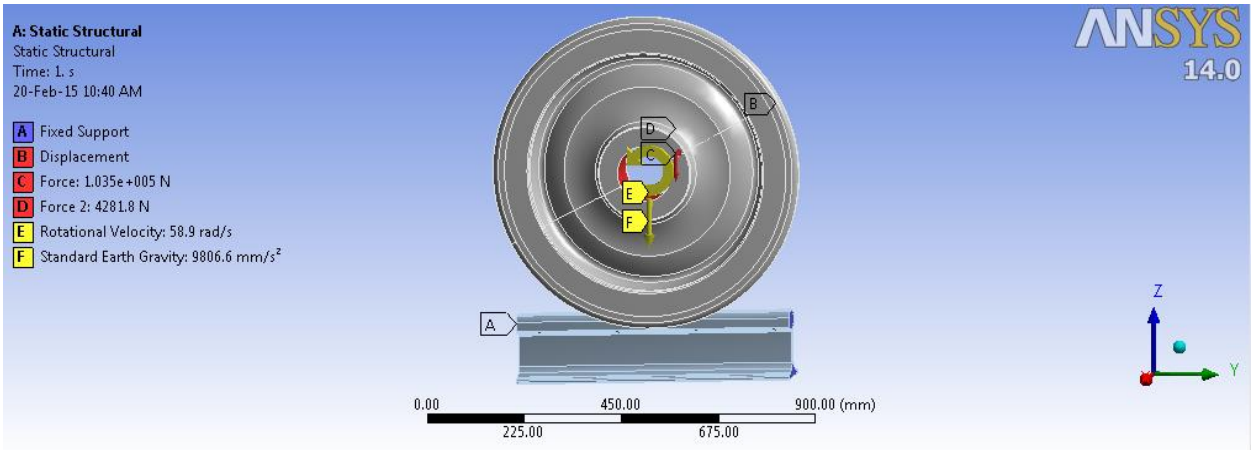

Figure 4.7: Loading and boundary conditions at transition curved track path.

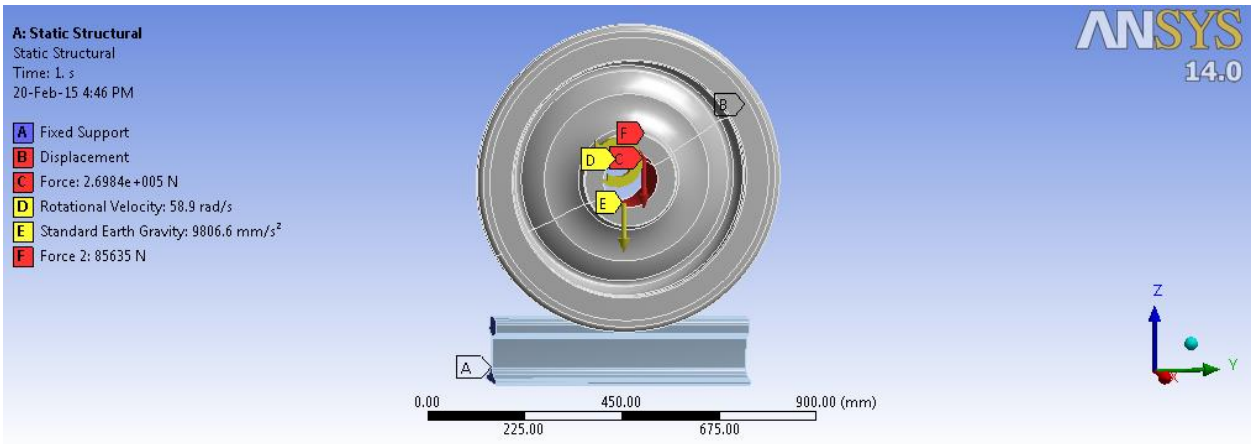

Figure 4.8: Loading and boundary conditions at circular curve track path.

4.5. Fatigue analysis and loading type

The Fatigue Analysis is based on the Stress Life approach.

4.5.2. Stress Life (S-N):

The stress life is concerned with total life and does not distinguish between initiation and propagation. In terms of cycles, Stress Life is based on S-N curves (Stress – Cycle curves) and has traditionally dealt with relatively high numbers of cycles and therefore addresses High Cycle Fatigue (HCF), greater than 10^5 cycles inclusive of infinite life [47].

Stress-life curves are assumed to follow a power relationship.

$$\frac{\Delta\sigma}{2} = \sigma_f (2N_f)^b \quad (4.3)$$

Here,

$\Delta\sigma/2$ is stress amplitude

N_f is cycles to failure.

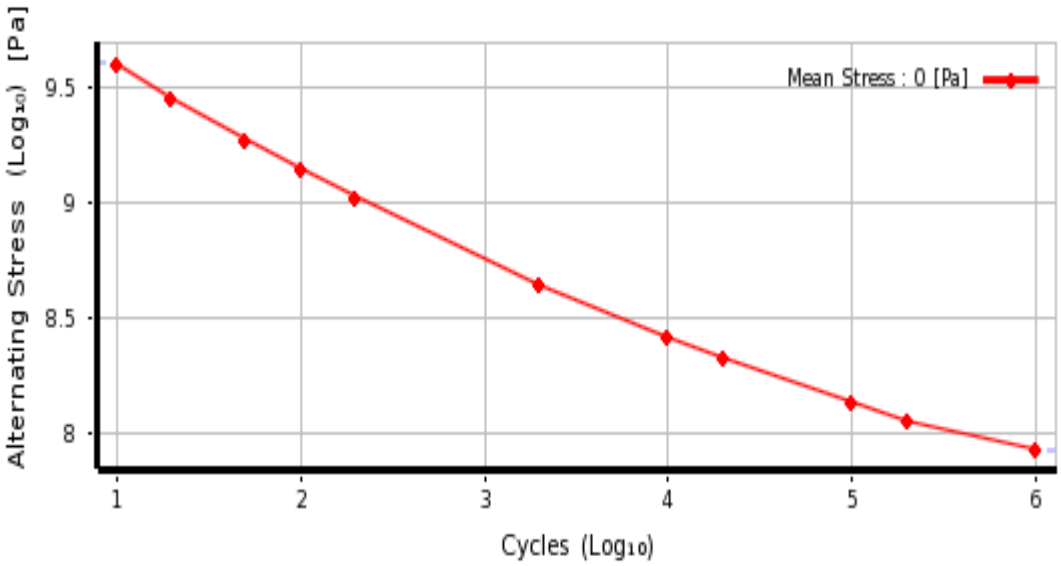

Figure 4.9: Stress life (S-N) diagram

4.5.3. Loading type:

Since the load created on the wheel is assumed quasi-static loads, then constant amplitude and proportional loading is used [39]. Loading is of constant amplitude because only one set of FE stress results along with a loading ratio is required to calculate the alternating and mean values. The loading ratio is defined as the ratio of the second load to the first load. Loading is proportional since only one set of FE results are needed (principal stress axes do not change over time). Since loading is proportional, looking at a single set of FE results can identify critical fatigue locations.

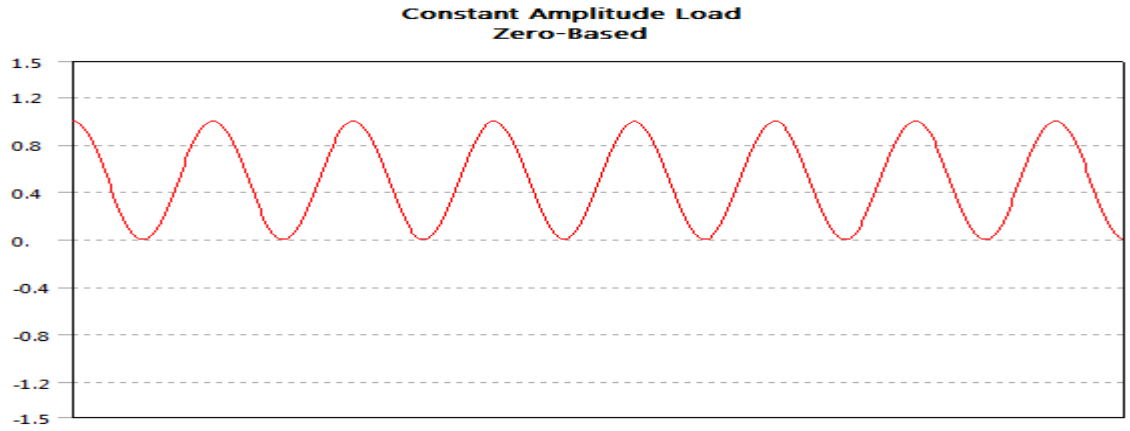

Figure 4.10: Zero-based loading response.

4.5.4. Mean stress correction for stress life:

If the loading is other than fully reversed, a mean stress exists and may be accounted for by using a mean stress correction. For this analysis Gerber method is used. And it is given by;

$$\frac{\sigma_{alt}}{S_{End-limit}} + \left(\frac{\sigma_{mean}}{S_{ult-strength}}\right)^2 = 1 \qquad (4.3)$$

$$\therefore \sigma_{alt} = \left(1 - \left(\frac{\sigma_{mean}}{S_{ult-strength}}\right)^2\right) S_{End-limit}$$

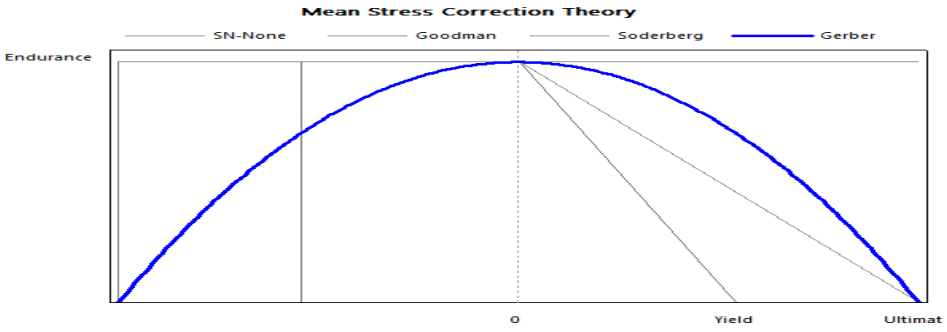

Figure 4.11: Mean stress correction (Gerber's diagram).

CHAPTER FIVE

RESULTS AND DISCUSSIONS

5.1. Results for stress-life fatigue analysis type:

5.1.1 Fatigue life:

This result contour plot shows us the available life for the given fatigue analysis. If loading is of constant amplitude, this represents the number of cycles until the part will fail due to fatigue.

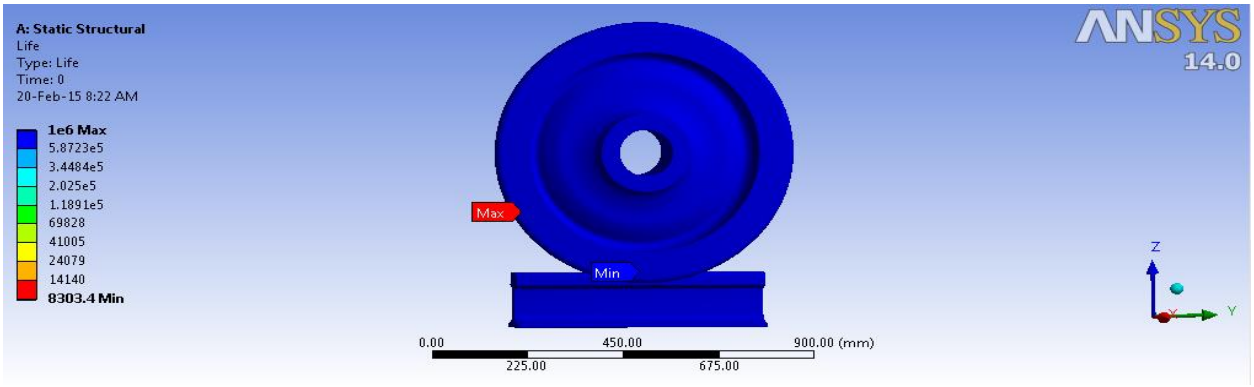

(a)

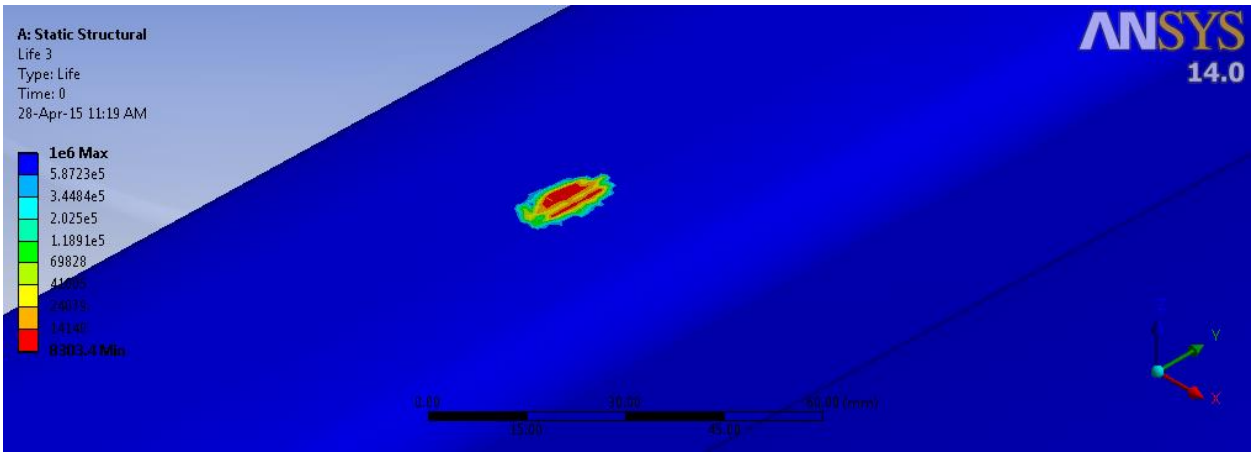

(b)

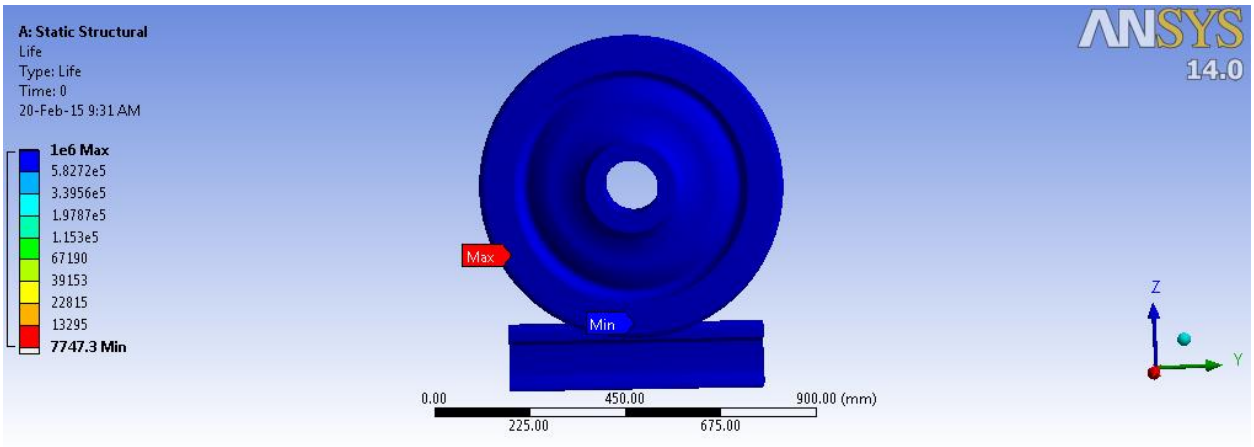

(d)

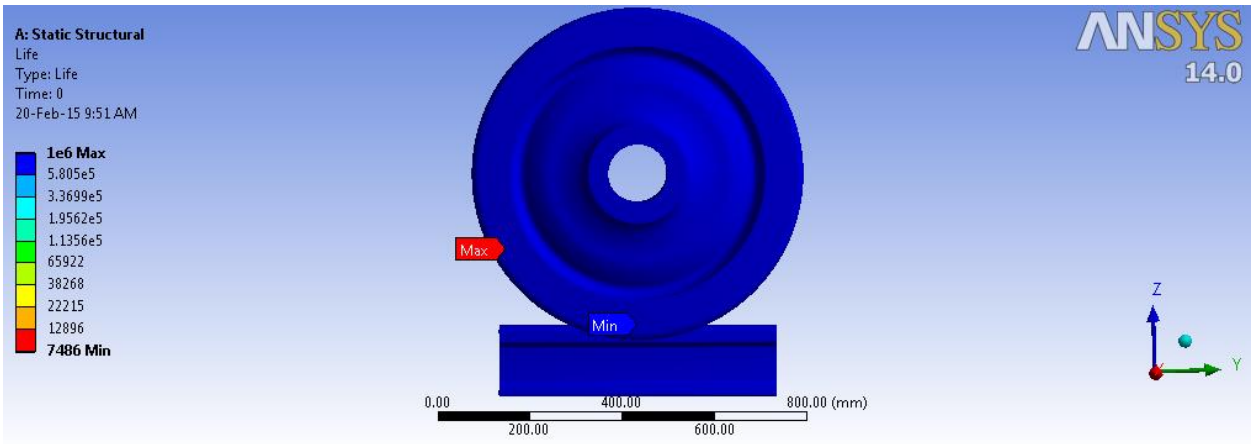

(e)

Figure 5.1: counter plot of fatigue life at the wheel-rail rolling contact at the straight track path. (a) at μ = 0.15, (b) at rail rolling contact, (d) at μ = 0.3, and (e) at μ = 0.6

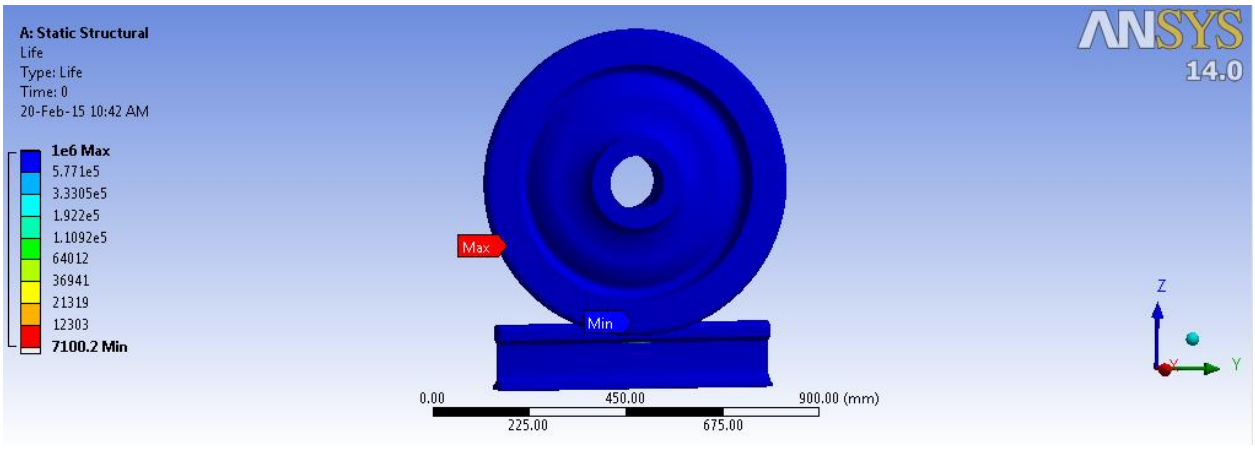
A: Static Structural
Life
Type: Life
Time: 0
20-Feb-15 10:42 AM
1e6 Max
5.771e5
3.3305e5
1.922e5
1.1092e5
64012
36941
21319
12303
7100.2 Min
Max
Min
ANSYS
14.0
0.00
450.00
900.00 (mm)
225.00
675.00
Z
Y

(a)

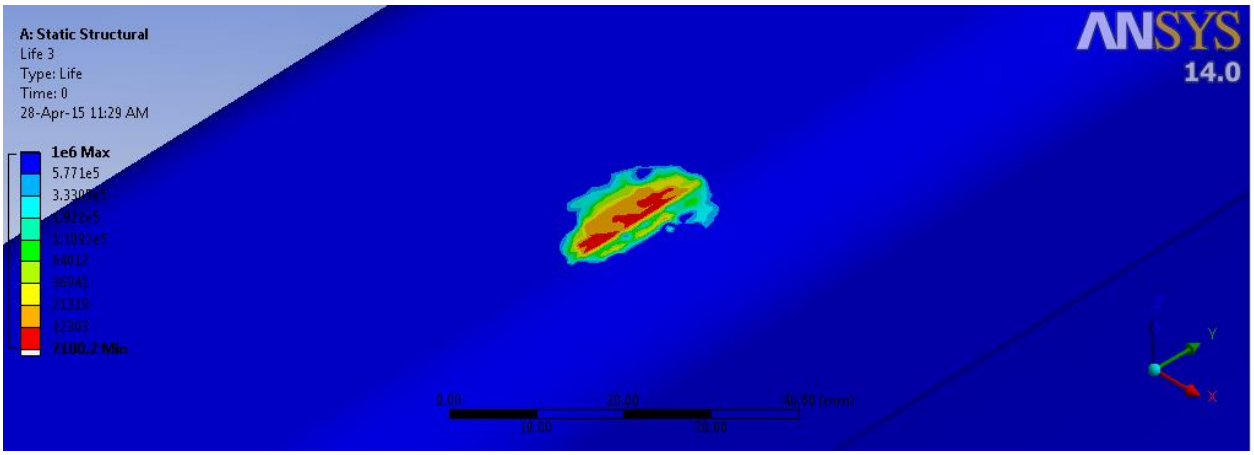
A: Static Structural
Life 3
Type: Life
Time: 0
28-Apr-15 11:29 AM
1e6 Max
5.771e5
7100.2 Min
ANSYS
14.0
Y
X

(b)

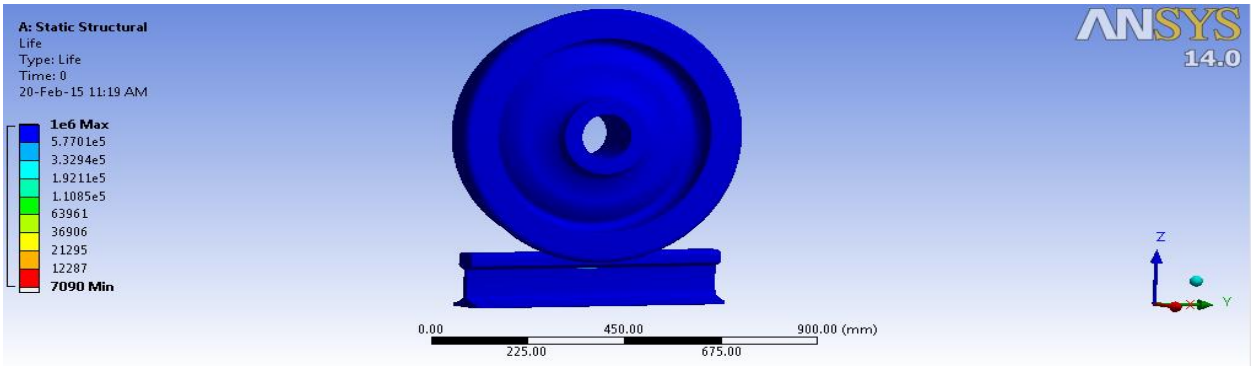
A: Static Structural
Life
Type: Life
Time: 0
20-Feb-15 11:19 AM
1e6 Max
5.7701e5
3.3294e5
1.9211e5
1.1085e5
63961
36906
21295
12287
7090 Min
ANSYS
14.0
0.00
450.00
900.00 (mm)
225.00
675.00
Z
Y

(d)

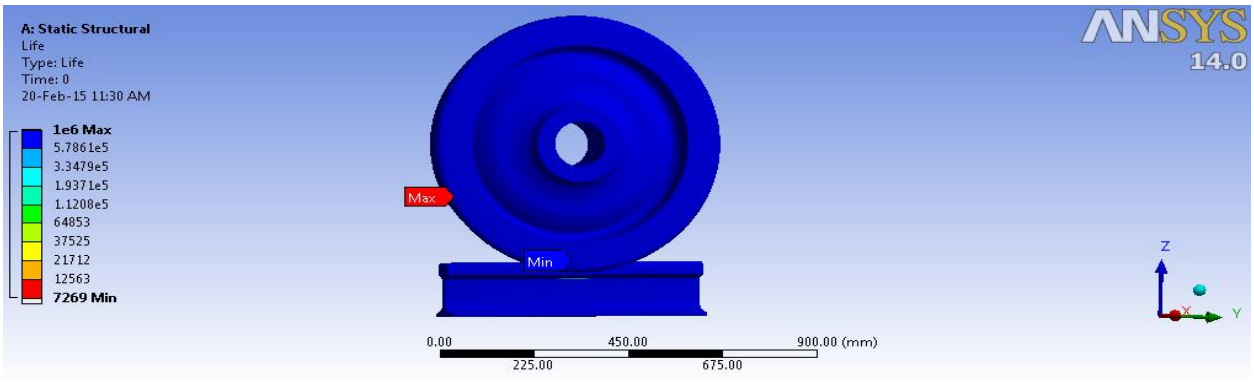

(e)

Figure 5.2: counter plot of fatigue life at the wheel-rail rolling contact at transition curve track path. (a) at μ = 0.15, (b) at wheel rolling contact, (c) at rail rolling contact, (d) at μ = 0.3, and (e) at μ = 0.6.

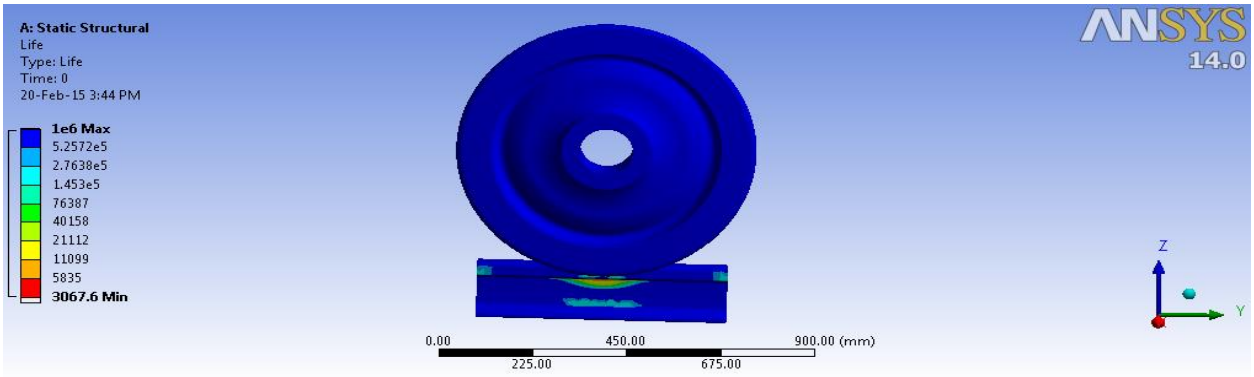

(a)

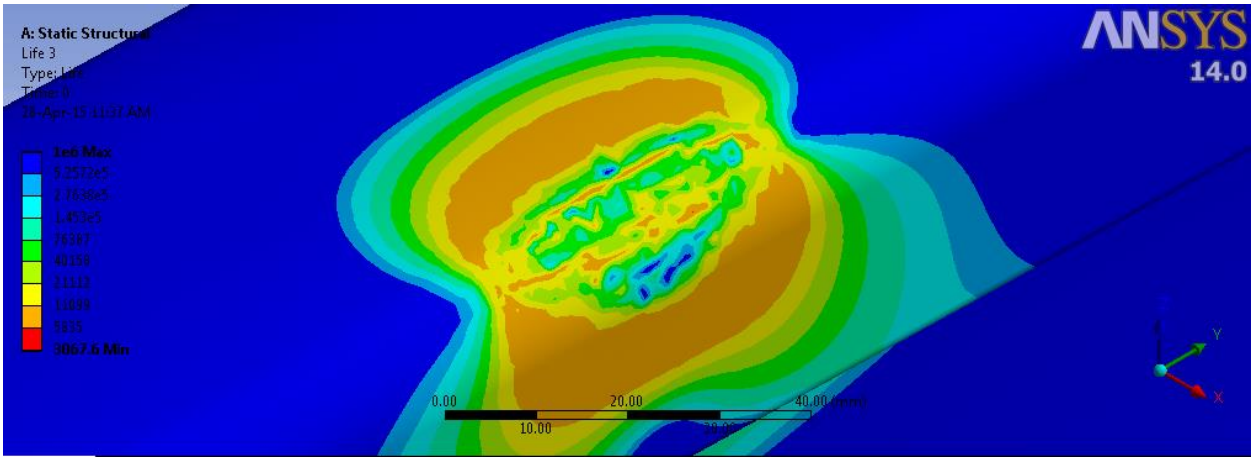

(b)

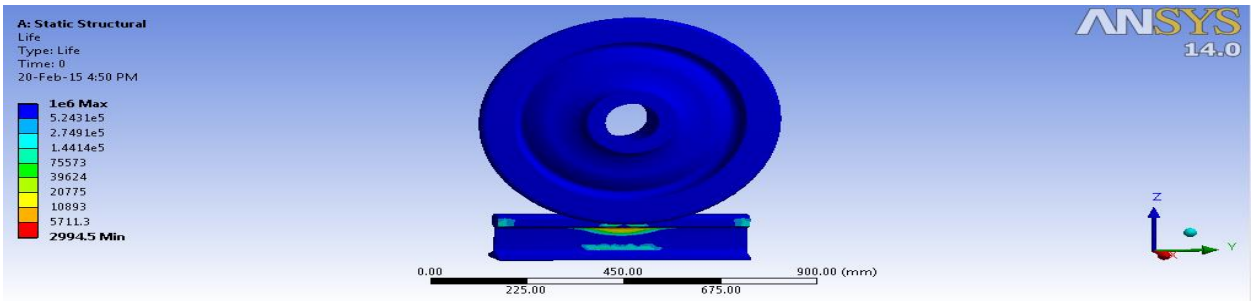

(d)

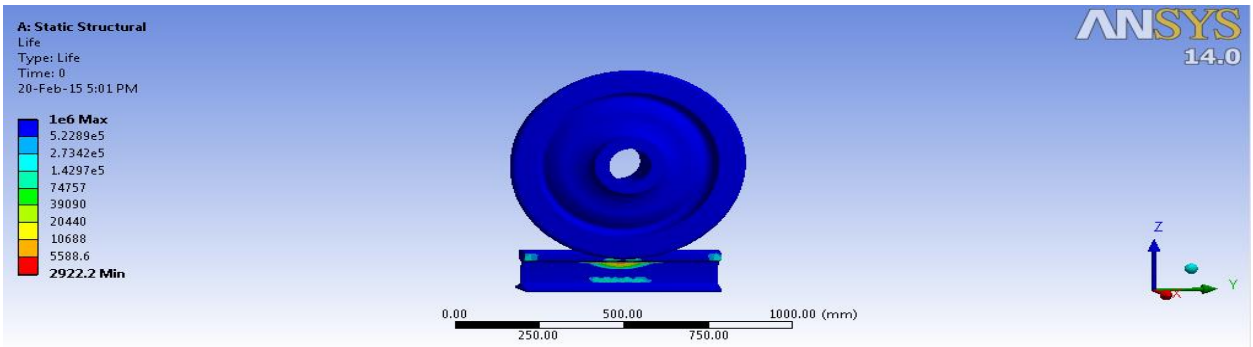

(e)

Figure 5.3: counter plot of fatigue life at the wheel-rail rolling contact at circular curve track path. (a) At μ = 0.15, (b) at the root flange of the wheel (c) at the gauge corner of the rail, (d) at μ = 0.3, and (e) at μ = 0.6.

5.1.3. Equivalent Alternating stress:

The equivalent alternating stress contour plot is the stress to query the S-N curve. Thus in a fatigue analysis, the equivalent alternating stress can be thought of as the last calculated quantity before determining the fatigue life. The usefulness of this result is that in general it contains all of the fatigue related calculations independent of any fatigue material properties. Some mean stress theories use static material properties such as tensile strength so Equivalent Alternating Stress may not be totally devoid of material properties. This result is not applicable to Strain Life or Stress life with non-constant amplitude fatigue loading due to the fact multiple SN queries per location are required and thus no single equivalent alternating stress exists.

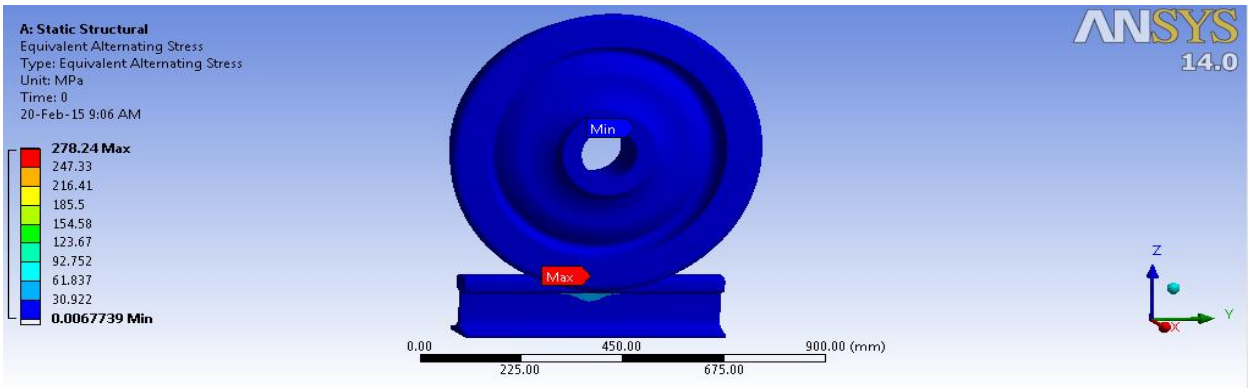
A: Static Structural
Equivalent Alternating Stress
Type: Equivalent Alternating Stress
Unit: MPa
Time: 0
20-Feb-15 9:06 AM
278.24 Max
247.33
216.41
185.5
154.58
123.67
92.752
61.837
30.922
0.0067739 Min
Min
Max
0.00
450.00
900.00 (mm)
225.00
675.00
ANSYS
14.0
Z
Y
X

(a)

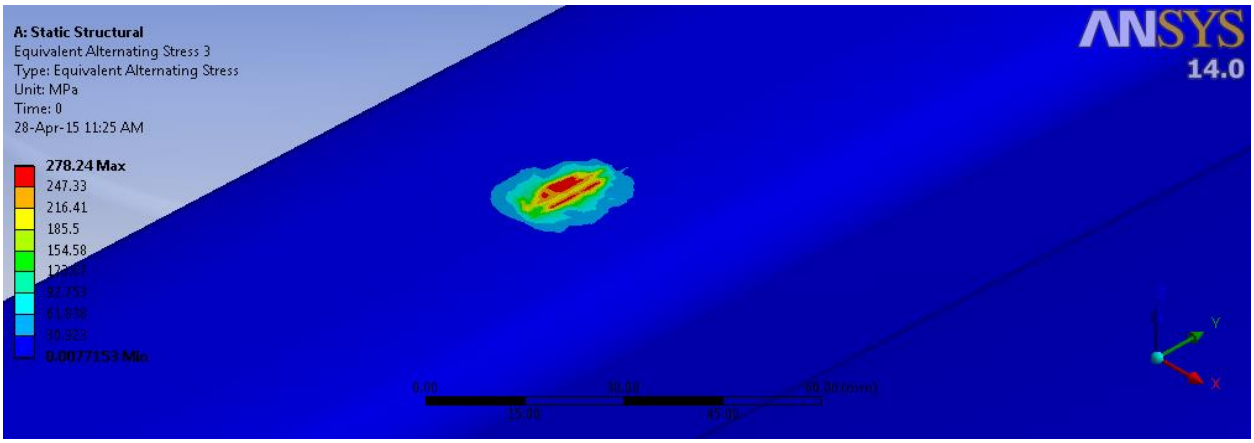
A: Static Structural
Equivalent Alternating Stress 3
Type: Equivalent Alternating Stress
Unit: MPa
Time: 0
28-Apr-15 11:25 AM
278.24 Max
247.33
216.41
185.5
154.58
0.0077153 Min
ANSYS
14.0
Y
X

(b)

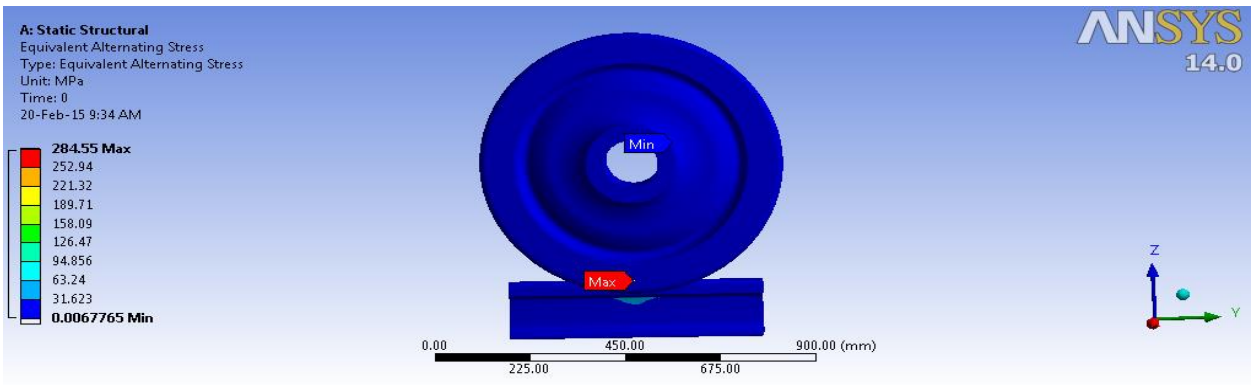
A: Static Structural
Equivalent Alternating Stress
Type: Equivalent Alternating Stress
Unit: MPa
Time: 0
20-Feb-15 9:34 AM
284.55 Max
252.94
221.32
189.71
158.09
126.47
94.856
63.24
31.623
0.0067765 Min
Min
Max
0.00
450.00
900.00 (mm)
225.00
675.00
ANSYS
14.0
Z
Y

(d)

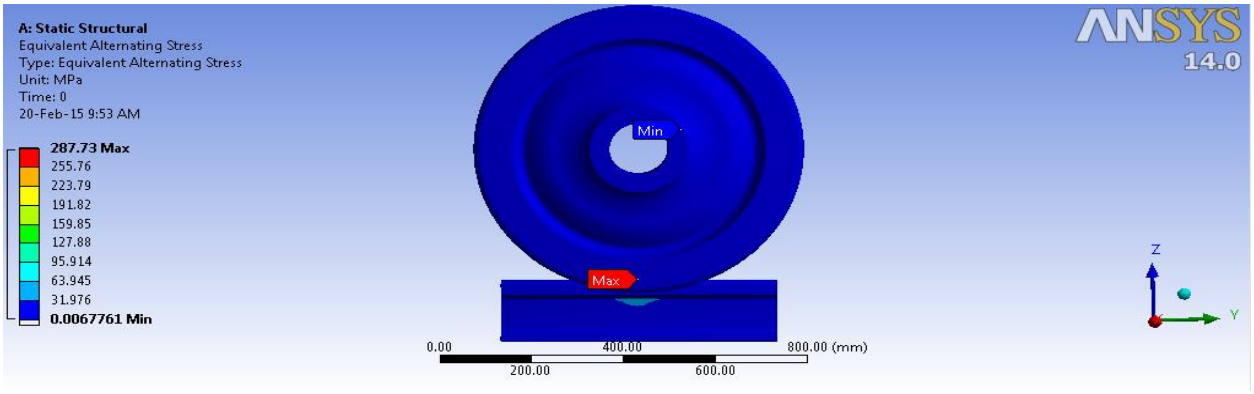

(e)

Figure 5.4: counter plot of equivalent alternating stress at the wheel-rail rolling contact at straight track path. (a) at μ = 0.15, (b) at rail rolling contact, (d) at μ = 0.3, and (e) at μ = 0.6

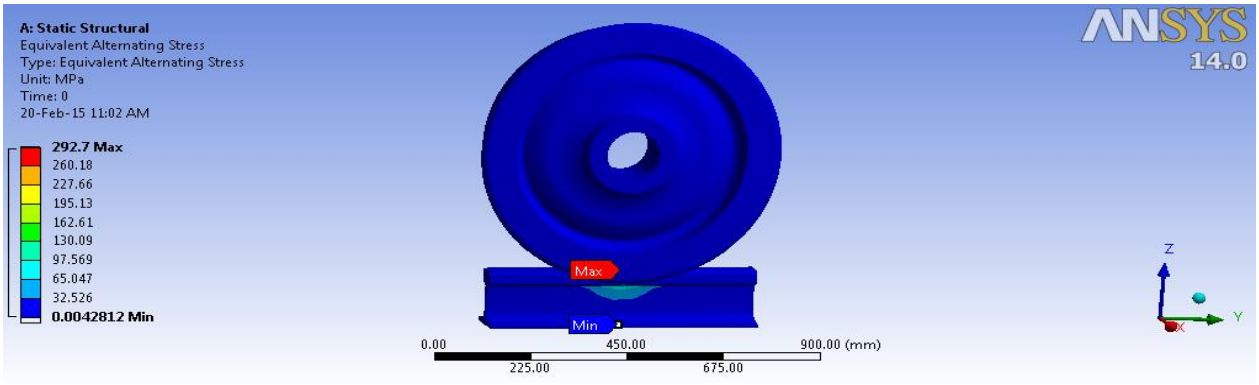

(a)

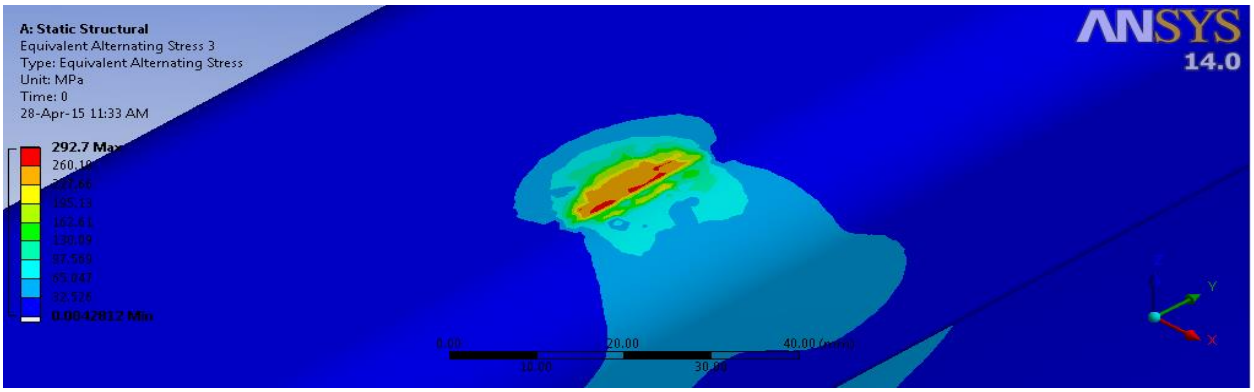

(b)

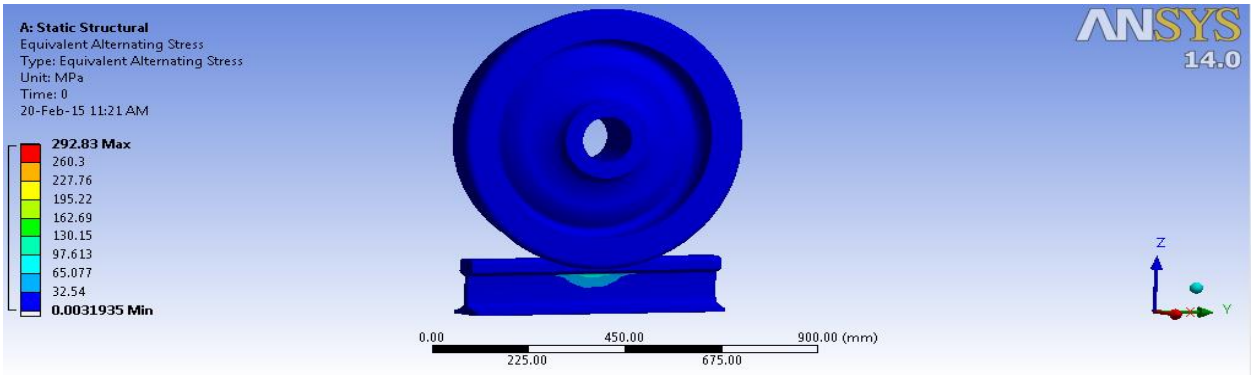

(d)

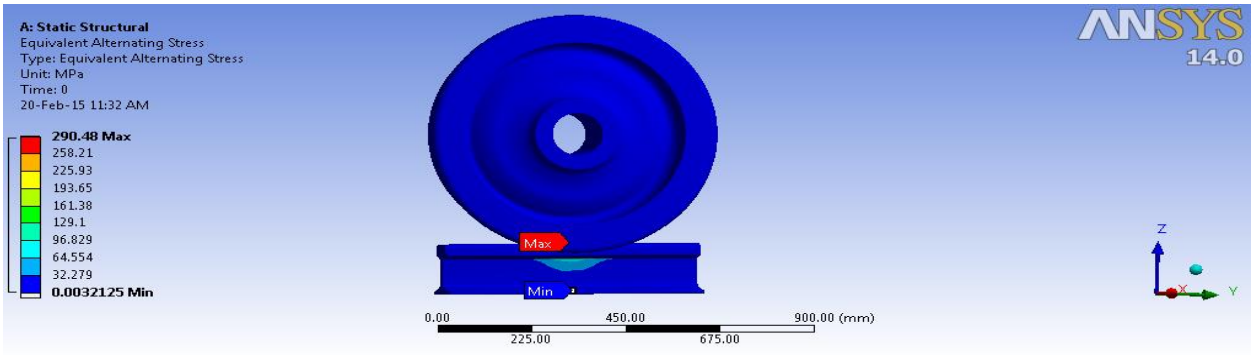

(e)

Figure 5.5: counter plot of equivalent alternating stress at the wheel-rail rolling contact at transition curve track path. (a) at μ = 0.15, (b) at rail rolling contact, (d) at μ = 0.3, and (e) at μ = 0.6

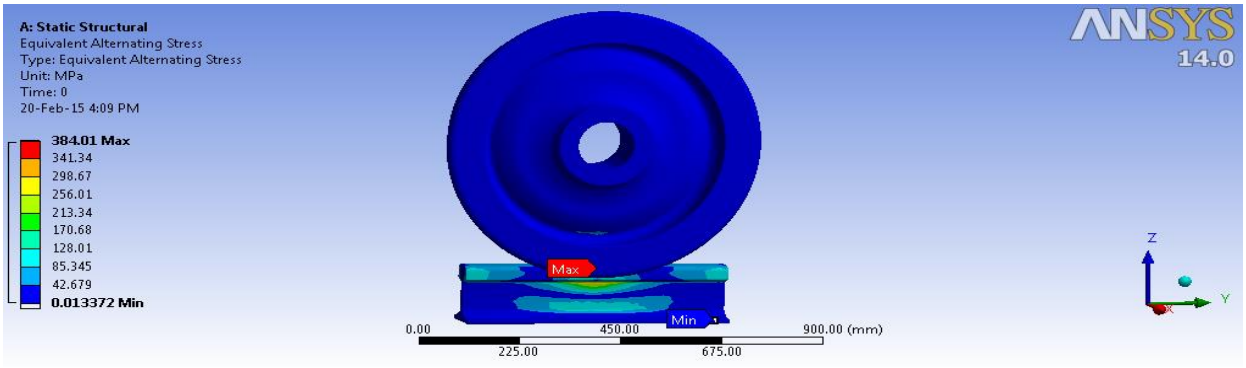

(a)

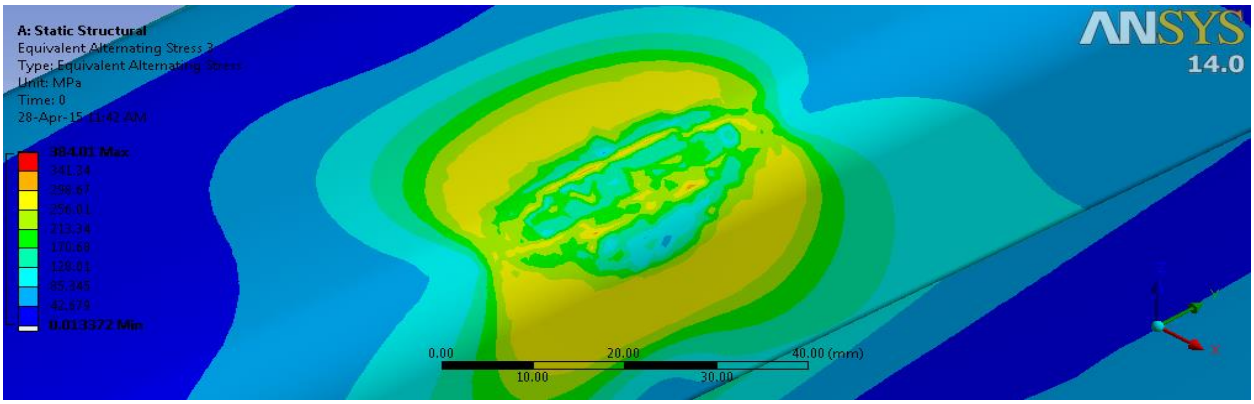

(b)

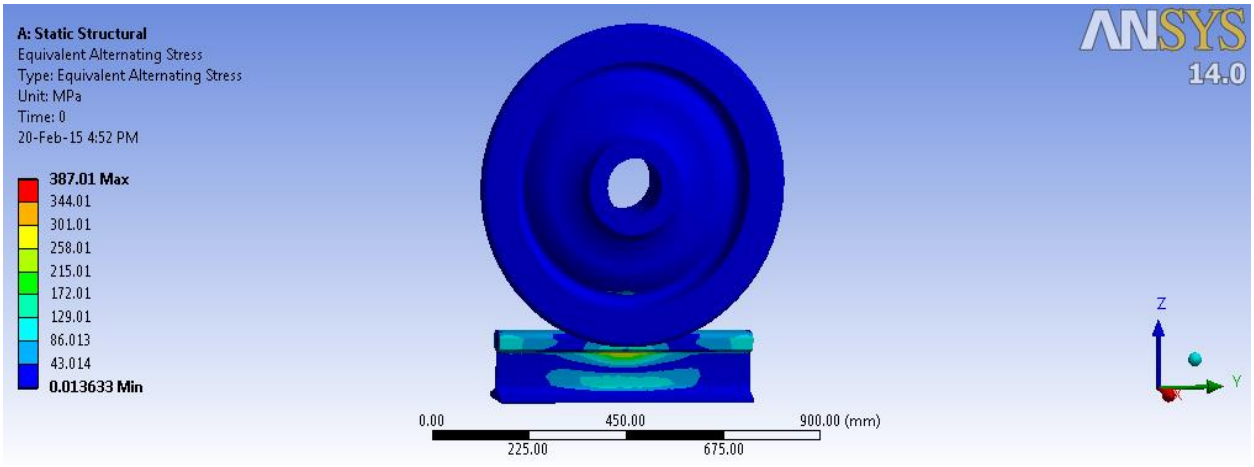

(d)

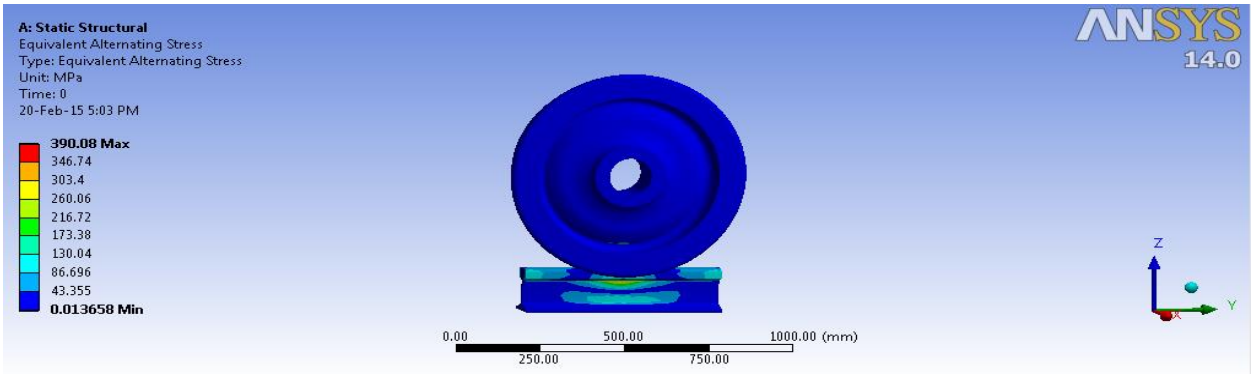

(e)

Figure 5.6: counter plot of equivalent alternating stress at the wheel-rail rolling contact at circular curve track path. (a) at μ = 0.15, (b) at rail gauge corner (d) at μ = 0.3, and (e) at μ = 0.6.

5.1.3. Equivalent Elastic strain:

This counter plot shows the deformation of the wheel/rail steel material at the rolling contact.

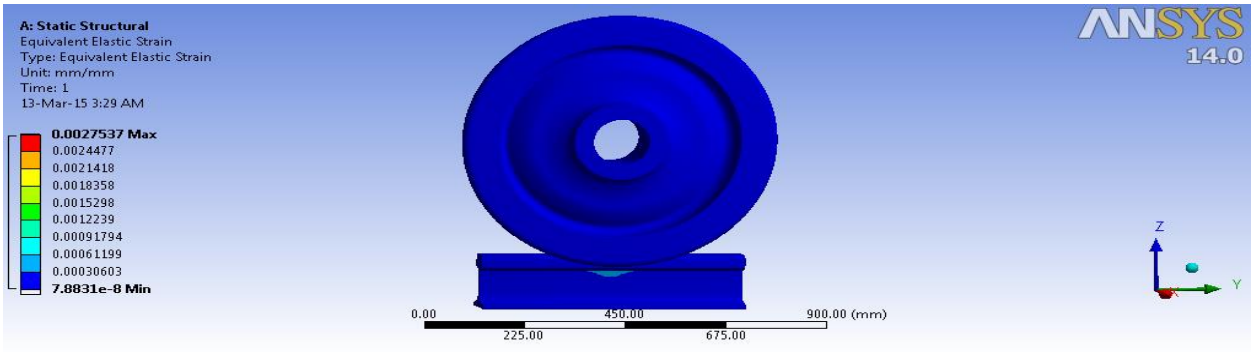

(a)

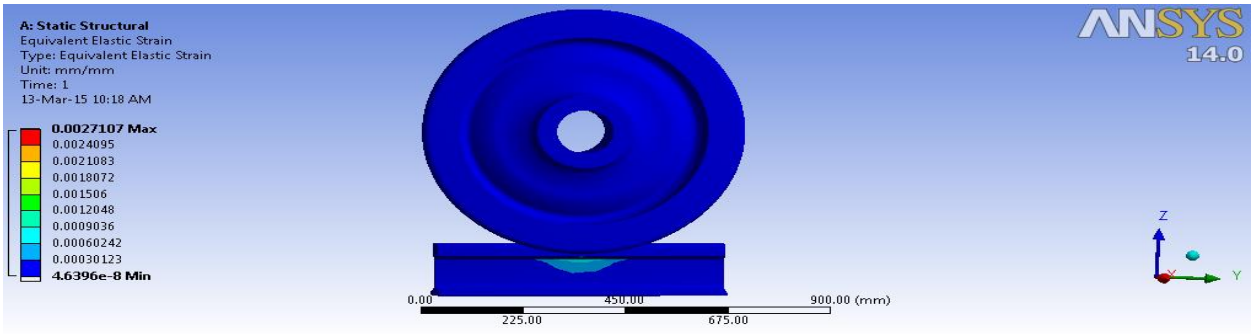

(b)

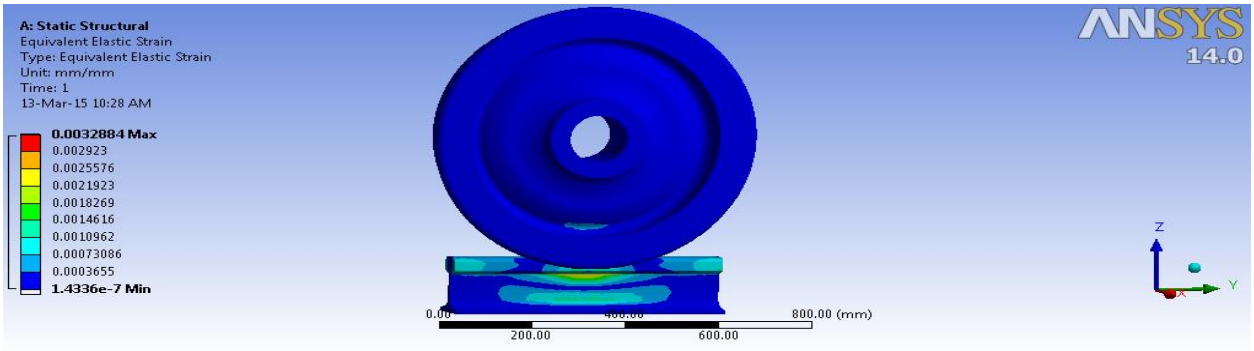

(c)

Figure 5.7: Equivalent elastic strain. (a) at straight, (b) at transition, and (c) at circular curve track

5.1.4. Fatigue sensitivity:

This plot shows how the fatigue results change as a function of the loading at the critical locations on the scoped region. Sensitivity may be found for life, damage, or factor of safety. If we set the lower and upper fatigue sensitivity limits to 50% and 150% respectively, and our scale factor is 1, this result will plot the data points along a scale ranging from a 0.5 to a 1.5 scale factor.

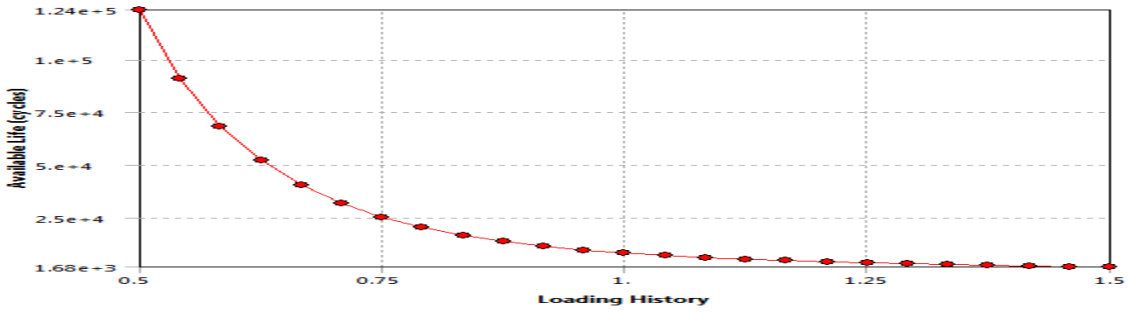

(a)

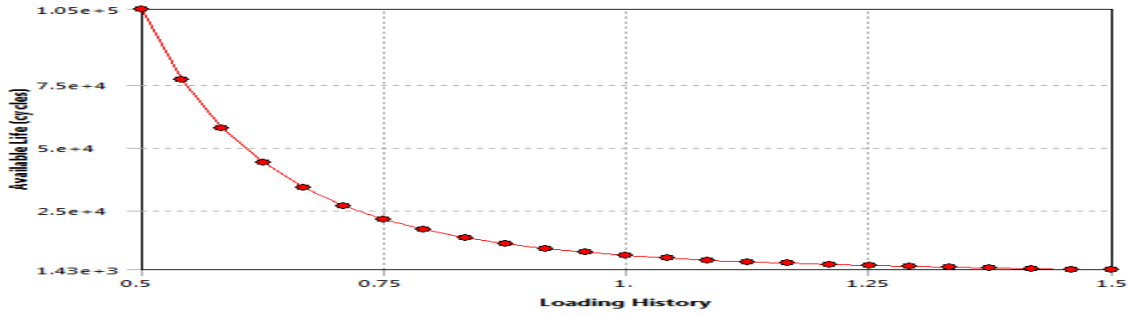

(b)

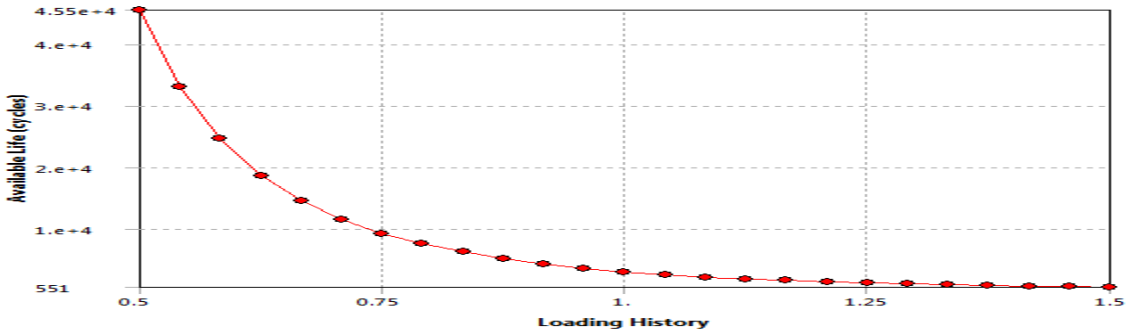

(c)

Figure 5.8: Fatigue sensitivity at the wheel-rail rolling contact. (a) at straight track, (b) at transition curve track, and (c) at circular curve track path.

5.2. Result discussions

5.2.1. Fatigue life versus Equivalent alternating stress:

In a Stress Life fatigue analysis, one always needs to query the S-N curve to relate the fatigue life to the stress state. Thus the "equivalent alternating stress" is the stress used to query the fatigue S-N curve after accounting for fatigue loading type, mean stress effects, multiaxial effects, and any other factors in the fatigue analysis.

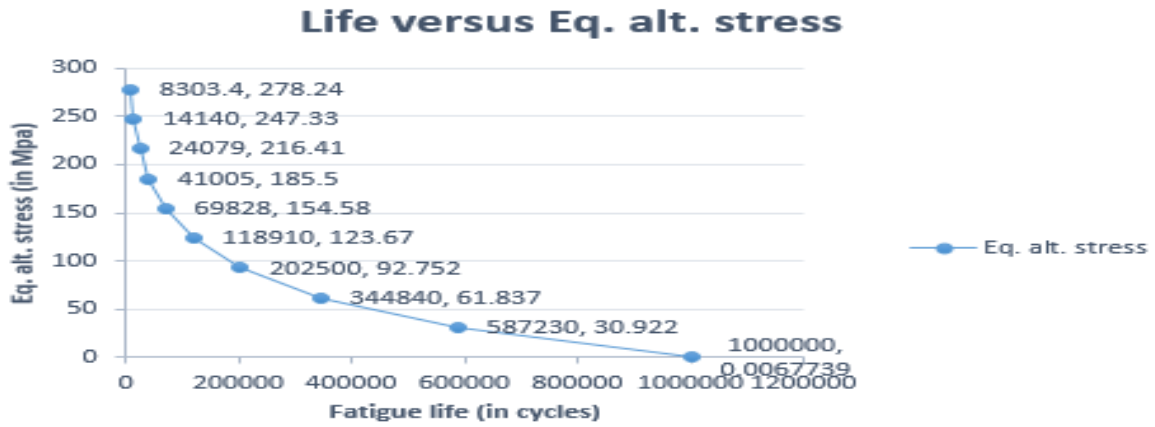

Figure 5.9: Fatigue life versus equivalent alternating stress at the rail rolling contact at straight track path.

5.2.3. Effect of track conditions on RCF at the wheel-rail contact

From the stress-life fatigue analysis, the obtained fatigue results at constant coefficient of friction and constant axle load indicate the track condition is greatly affected the wheel-rail rolling contact fatigue. The life cycles at the rail rolling contact at the circular curve track path is relatively smaller when compared with the life at the straight tack path. The minimum fatigue life of rail rolling contact at straight, transition curve and circular curve track paths are presented here in table 5.2.

Table 5.2: Effect of track conditions on fatigue life at the rail rolling contact.

Fatigue result	At straight track	At transition curve	Circular curve track
Life	8303 cycles	7100.2 cycles	3067.6 cycles

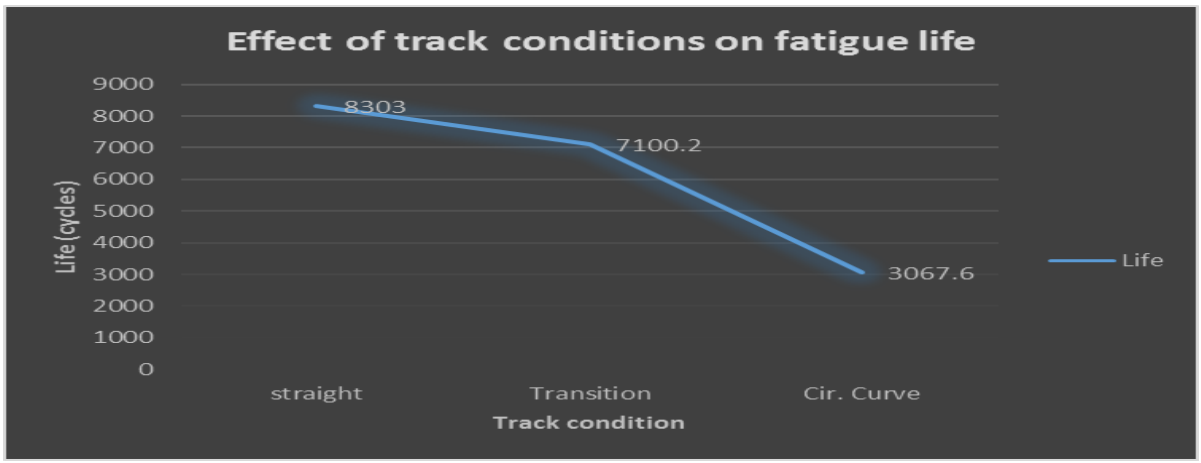

Figure 5.10: Effect of track condition on fatigue life at the rail rolling contact.

5.2.4. The effect of coefficient of friction, (μ) on the fatigue life at the wheel-rail rolling contact

The fatigue results at the wheel- rail rolling contact at the assumed three different coefficient of friction, μ (0.15, 0.3, 0.6) show that the coefficient of friction, μ has signifficant effect on fatigue life of wheel-rail rolling contact. The minimum life at the wheel-rail rolling contact at the three assumed coefficient of friction, μ in both fatigue analysis (stress and strain life) is summerized in table 5.3.

Table 5.3: Effect of coefficient of friction on fatigue life at the rail rolling contact

Coe. Friction, μ	Straight track	Transition curve track	Circular curve track
	Fatigue life (in cycles)	Fatigue life (in cycles)	Fatigue life (in cycles)
0.15	8303	7100.2	3067.6
0.3	7747.3	7090	2994.5
0.6	7486	7269	2922.2

Table 5.4: Effect of coefficient of friction on eqivalent alternating stress at the rail rolling contact.

Coe. Friction, μ	Straight track	Transition curve track	Circular curve track
0.15	278.24Mpa	292.7Mpa	384.01Mpa
0.3	284.55Mpa	292.83Mpa	387.01Mpa
0.6	287.73Mpa	292.48Mpa	390.08Mpa

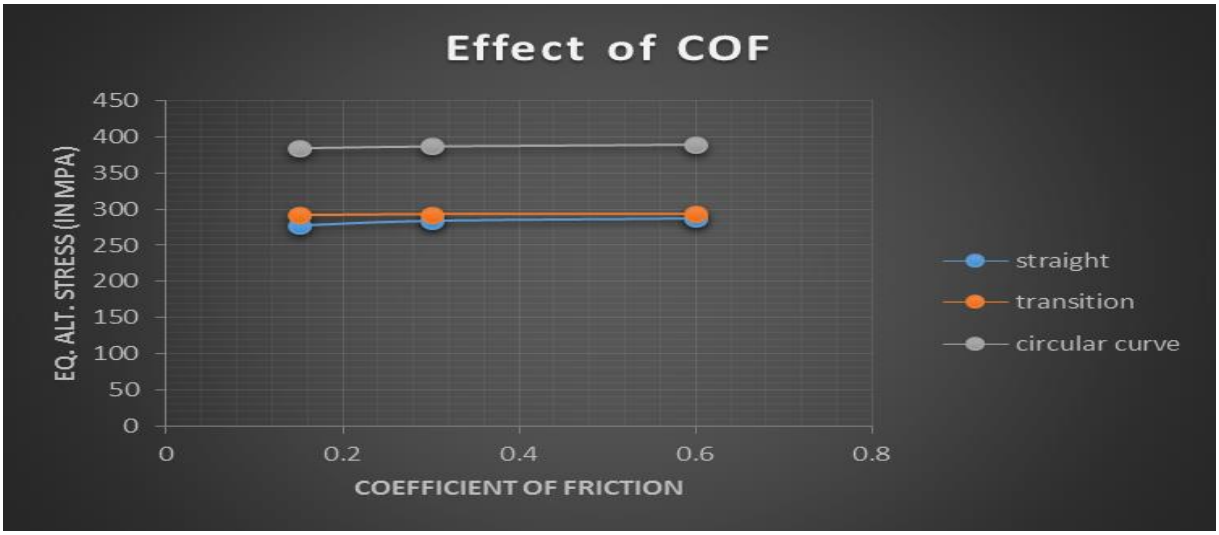

Figure 5.11: Effect of coefficient of friction on equivalent alternating stress at the wheel-rail rolling contact at different track conditions.

CHAPTER SIX

CONCLUSION, RECOMMENDATIONS, AND FUTURE WORKS

6.1. Conclusion:

The thesis presents analysis of rolling contact fatigue at the wheel-rail interface. A three-dimensional finite element model is used for the wheel-rail rolling contact fatigue analysis. The wheel-rail assembly geometry is created in CATIA software. The finite element program ANSYS workbench is used to model the rolling contact fatigue analysis and used to simulate the loading and boundary conditions of the wheel-rail rolling contact. The fatigue analysis is based on the stress life approach. The effect of coefficient of friction and track conditions on fatigue failure at the wheel-rail rolling contact are investigated in detail. The obtained results from the present investigation indicate that the rolling contact coefficient of friction has significant effect on the fatigue life of the wheel-rail rolling contact and the track condition has a great effect on the fatigue life of the wheel-rail rolling contact. At constant axle load and coefficient of friction the minimum fatigue life at the wheel-rail rolling contact is at the circular curve track path. The effect of mean stress correction is considered during the FEA analysis. The Gerber method is used throughout the FEA. At straight track path the minimum rolling contact fatigue life is shown at the center of the rail head and wheel tread center. Whereas, at the circular curve track path the minimum rolling contact fatigue life is formed at the rail corner gauge and at the wheel root flange. The maximum equivalent alternating stresses and minimum fatigue life at the rail rolling contact at different track conditions (at straight, transition curve, circular curve track path) at constant rolling contact coefficient of friction, ($\mu = 0.3$) are 284.55Mpa, 292.83Mpa, 387.01Mpa and 7747.3 cycles, 7090 cycles, 2994.5 cycles respectively. These results are useful in fatigue resistance design and inspections for AA LRT in Ethiopia.

6.2. Recommendation

Based on the finite element analysis (fatigue analysis), the rolling contact fatigue at the wheel-rail interface indicate that the amplitude/alternating stresses are below the fatigue strength (or endurance limit) of the wheel/rail steel material at all track conditions. Fatigue strength or endurance limit is the expression used to describe a property of materials that the amplitude (or range) of cyclic stress that can be applied to the material without causing fatigue failure [48]. Know that the endurance limit (S_e) or fatigue strength for steel materials is approximated by half of the ultimate tensile strength of the steel material; i.e. $S_e = 0.5*S_{ult}$, for $S_{ult} \leq 1400$ Mpa [49]. Therefore, based on the present thesis, the ultimate tensile strength, S_{ult} of the wheel/rail steel material is 880Mpa. Thus, the endurance limit or fatigue strength of the wheel/rail steel will be 440 Mpa. But the maximum amplitude/alternating stress at the wheel-rail rolling contact from the finite element analysis (or fatigue analysis) result is 390.08Mpa (i.e. at the circular track path); which is below the endurance limit, S_e = 440Mpa. This shows the wheel/rail rolling contact at all track conditions are at safe condition. Note that, the maximum alternating stress is at the minimum allowable circular curve radius 50m (circular curve track path). However, the rail rolling contact fatigue life at the circular curve track is relatively smaller as compared with the straight track path. At constant coefficient of friction, $\mu = 0.15$ the fatigue life at the rail rolling contact at straight, transition, circular curve track is 8303 cycles, 7100.2 cycles, and 3067.6 cycles respectively. Therefore, it is better to suggest or recommend to Ethiopian railway corporation (ERC); for reducing the potential development of rolling contact (RCF) defects and consequently the associated potential risk of rail failure:

- Install higher strength rail steels in the more critical track locations (at the circular curve track paths) to increase the allowable shear stress limits and to reduce plastic deformation.
- Regular inspections or crack testing using suitable methods of rails should be apply in all critical track regions.

6.3. Future Works:

The scope of the present thesis focus on the analysis rolling contact fatigue at the wheel-rail interface using finite element analysis ANSYS software. The fatigue analysis is based on the stress life approach by considering the mean stress effect. The fatigue analysis is performed by applying the mechanical loads to the wheel-rail contact at different track conditions (straight, transition and circular curve track paths) and considering the rolling contact coefficient of friction. The continuity of the thesis work will be:

1. The present thesis tried to predict the fatigue life at the wheel-rail rolling contact at different track conditions (i.e. at straight, transition and circular curve track path) using ANSYS software and it enable to oversees the effect of track condition and rolling contact coefficient of friction on fatigue life at the wheel-rail contact. Therefore, the results obtained from the FEA should be check experimentally using appropriate testing machine.
2. Thermo-mechanical fatigue analysis of railway wheel in sliding-rolling motion using finite element method (FEM). This helps to investigate the effect of thermal loads on fatigue life of wheel tread during slipping or sliding.
3. Predicting crack growth due to rolling contact fatigue with respect to stress intensity by assuming crack is already presented and detected on the wheel tread or rail head using appropriate software.
4. Investigating on fatigue failure prevention methods at the wheel-rail rolling contact.

REFERANCES

1. lihong wang, microstructure and residual stress state in the contact zone of rails and wheels, berlin university, 12 September 2002.
2. Dr.Richard Pankhurst, December 4,1906, Addis Ababa.
3. Crozet, Jean-Pierre. Françoise Faulkner-Trine, trans. The Franco-Ethiopian and Djibouto-Ethiopian Railway and "History". 2013. Accessed 12 Feb 2014.
4. Ethiosports, Track laying commences on section of Ethio-Djibouti Railway project, Published By Markos Berhanu On Sunday, May 11th 2014.
5. "Corporation discloses/Addis light rail project detail". The Ethiopian Herald. 10 March 2013. Archived from the original on 2013-03-11. Retrieved 2014-10-25.
6. "Addis Light Rail Progress". Railways Africa. 2 October 2013. Retrieved 2013-11-25.
7. Tournay HM, Mulder JM, The transition from the wear to the stress regime, Wear 1996.
8. Mann, J.Y., Bibliography on the fatigue of materials, components and structures, 1838-1950, 1970, Pergamon Press, Oxford, U.K., 316 pp.
9. Wöhler, A., Engineering, vol.11, 1871.
10. Lin, T.H., Micromechanics of crack initiation in high-cycle fatigue, Advances in Applied Mechanics, 1992, vol.29, pp.1-62.
11. Ekberg, A. & Kabo, E. “Fatigue of Railway Wheels and Rails under Rolling Contact and Thermal Loading-An Overview”, Wear, Vol.258, 2005, pp.1288-1300.
12. Magel, E., and Kalousek, J., The influence of creep forces on surface fatigue of wheels, 14th International Wheelset Congress, Orlando, FL.,2004.
13. Magel, E., and Kalousek, J., Martensite and contact fatigue initiated wheel defects, Proceedings from the 12th International Wheelset Congress, Quingdao, China, 1998.
14. Office of Rail Regulation (ORR). “Train Derailment at Hatfield: A Final Report by the Independent Investigation Board, (UK)” Health and Safety Executive, July 2006.

15. Miller, K., J. “Structural Integrity-Whose Responsibility?”, Proceedings of the Institute of the Mechanical Engineers, Part L: Journal of Material: Design and Application, Vol. 217, 2003, pp. 1-22.

16. Zakharov, S., M. & Goryacheva, I., G. “Rolling Contact Fatigue Defects in Freight Car Wheels”, Wear, Vol. 258, 2005, pp. 1142-1147.

17. Evans, J. & Iwnicki, S., D. "Vehicle Dynamics and Wheel/Rail Interface", Article from Rail Technology Unit Website at MMU.

18. Ekberg, A. & Kabo, E. “Fatigue of Railway Wheels and Rails under Rolling Contact and Thermal Loading-An Overview”, Wear, Vol.258, 2005, pp.1288-1300.

19. Davis, C., L. “Modelling and Detecting Damage (Wear and RCF) in Rails”, Prepared for Rail Safety and Standard Board, School of Engineering, University of Birmingham, 2003.

20. Olver, A., V. "The Mechanism of Rolling Contact Fatigue: An Update", Proceedings of the Institution of Mechanical Engineers, Part J: Journal of Engineering Tribology, Vol. 219, No. 5, 2005, pp. 313-330.

21. Ringsberg, J., W. “Life Prediction of Rolling Contact Fatigue Crack Initiation”, International Journal of Fatigue, Vol. 23, 2001, pp. 575-586.

22. Chue, C., H., Chung, H., H. , Lin, J., F. & Chou, C., C. “The Effect of Strain Hardened Layer on Pitting Formation During Rolling Contact”, Wear, Vol. 249, 2001, pp. 109-116.

23. Fletcher, D., I., Franklin, F., J. & Kapoor, A. “Image Analysis to Reveal Crack Development using a Computer Simulation of Wear and Rolling Contact Fatigue”, Fatigue & Fracture of Engineering Materials and Structures, Vol. 26, 2003, pp. 957-967.

24. Brennan, F., P. & Teh, L., S. “Determination of Crack-tip Stress Intensity Factors in Complex Geometries by the Composition of Constituent Weight Function Solutions”, Fatigue & Fracture of Engineering Materials & Structures, Vol. 27, No.1, 2004, pp. 1-7.

25. Barter, S., Molent, L., Goldsmith, N. & Jones, R. “An Experimental Evaluation of Fatigue Crack Growth”, Engineering failure analysis, Vol. 12, 2005, pp. 99-128.

26. Dixon, S., Edwards, R., S. & Jian, X. "Inspection of Rail Track Head Surfaces Using Electromagnetic Acoustic Transducers (EMATs)", Insight, Vol. 46, No. 6, 2004, pp. 32-330.

27. Y. Zhu, Adhesion in the wheel – rail contact under contaminated conditions, Licentiate thesis, KTH Royal Institute of Technology, 2011.

28. Rolling contact fatigue:Acomprenhesive review,U.S.department of transportation federal railroad administration, nov.2011.

29. Jean-Bernard Ayasse and Hugues Chollet. Chapter 4: Wheel-rail contact. In Simon Iwnicki, editor, Handbook of Railway Vehicle Dynamics, pages 209–237. CRC Press, Taylor & Francis Group, Boca Raton, FL, 2006.

30. Johnson KL. The strength of surfaces in rolling contact. Proc Inst Mech Eng IMechE 1989.

31. Stone DH, Moyar GJ. Wheel shelling and spalling—an interpretive review. In: Rail transportation 1989. ASME; 1989. p. 19–31.

32. Marais JJ. Wheel failures on heavy haul freight wheels due to subsurface effects. Proceedings of 12th international wheelset congress, Qingdao, China; 1998. p. 306–314.

33. Mutton PJ, Epp CJ, Dudek J. Rolling contact fatigue in railway wheels under high axle loads. Wear 1991.

34. Ekberg A, Marais J. Effects of imperfections on fatigue initiation in railway wheels. IMechE J Rail Rapid Trans 1999.

35. Yongming liu, Brant atrat man, Sankaran Mahadevan, fatigue crack initiation life prediction of railroad wheels, international journal of fatigue 28 ,2006, pp.747-756.

36. Sumant Patel, Dr.A.V.Gohil, wheel-rail contact fatigue, international journal of engineering research and application, vol.3, issue2, March-April, 2013, pp.980-983.

37. V.palaniselvam, S.sabareesan, S.karthik, design and analysis of train wheel during rolling action, international journal of software and hardware research in engineering, vol.2,issue5, may 2014.

38. Taek young kim, Ho kyungkim, three dimensional elastic plastic finite element analysis for wheel-rail rolling contact fatigue, seoul national university of science and technology, vol.6, number3, jun-july 2014.

39. N.A.Akeel, Z. sajuri and A.K.Ariffin, analysis of rolling contact fatigue damage initiation at the wheel-rail interface, Australia journal of basic and applied science 5(12), 2011,pp. 937-945.

40. K. Dan Van, B. Griveau, and O. Message, "On a new multiaxial fatigue limit criterion: Theory and Application, in Biaxial and Multiaxial Fatigue," European Group on Fracture, EGF Publication 3, Mech. Eng. Publ., London, pp. 479-496, 1989.

41. A.H. Wickens. Fundamentals of Rail Vehicle Dynamics: Guidance and Stability. Swets & Zeitlinger, Lisse, Netherlands, 2003.

42. George Bibel. Train Wreck: The Forensics of Rail Disasters. Johns Hopkins University Press, Baltimore, MD, 2012.

43. Andersson, E., Berg, M. and Stichel, S. (1998) "Rail Vehicle Dynamics, Fundamentals and Guidelines", Royal Institute of Technology (KTH), Stockholm, Sweden.

44. The University of Southern Queensland, Horizontal alignment: Transition curve, 2000-2001.

45. EN 13262 railway applications,wheelsets and bogies wheels product requirements,issue 01/2006.

46. Prachi Katheriya, veerendra Kumar, Anshul Choudhary, Raji Nareliya, An Investigation of effects of axle load and train speed atbrail joint using finite element method, international journal of research in engineering and technology, vol.3,,issue8, Aug 2014.

47. Raymond L. Browell, P.E, Predicting fatigue life with ansys workbench, International ANSYS conference, may 2-4, 2006.

48. Beer, Ferdinand P, E.Russel Johnston, Mechanics of materials (2^{nd} ed), Jr. 1992.

49. Dr. Ala Hijazi, Shigley's Mechanical engineering design, 9th ed, chapter six, class notes.

50. China railway group limited, preliminary design description for Addis Ababa E-W and N-S (phase one) light rail transit project in Ethiopia.

51. China Railway Group (CRECG) Project Manager Office for Light Rail Project of Ethiopia, Technical Specifications of Vehicles, July 2013.